# FURTHER EXPERIMENTAL INVESTIGATIONS INTO ELECTRIC CHARGING IN FUEL FILTRATION

by

ANTHONY H. WEXLER

B.S., University of California, Berkeley
(1976)

SUBMITTED IN PARTIAL FULFILLMENT
OF THE REQUIREMENTS FOR THE
DEGREE OF

MASTER OF SCIENCE

at the

MASSACHUSETTS INSTITUTE OF TECHNOLOGY

February 1978

Signature redacted

Signature of Author . . . . . .
Department of Mechanical Engineering, February 3, 1978

Signature redacted

Certified by . . . . . .
Thesis Supervisor

Signature redacted

Accepted by . . . . . .
Chairman, Department Committee on Graduate Students

2

# FURTHER EXPERIMENTAL INVESTIGATIONS INTO ELECTRIC CHARGING IN FUEL FILTRATION

by

ANTHONY H. WEXLER

Submitted to the Department of Mechanical Engineering
on February 3, 1978 in partial fulfillment of the
requirements for the Degree of Master of Science

## ABSTRACT

Experimental data are presented on the charging emf's developed by various Millipore filters when kerosine doped with Shell ASA-3 is used as the working fluid. The data is compared with the theory of Huber and Sonin and good agreement is found. From this comparison, we estimate the mobilities of the ions of ASA-3 in kerosine.

Thesis Supervisor: Ain A. Sonin
Title: Professor of Mechanical Engineering

## ACKNOWLEDGEMENTS

I would like to thank my advisor, Professor Ain Sonin, for his guidance and suggestions on my research during my stay at MIT. I would also like to thank Peter Huber for his suggestions and help, and Cindy Polansky for her patience with my handwriting. For her moral support and loving care, I would like to thank Rebecca Stein. I would also like to thank Steve Anderka, Mary Lubischer, Phoebe Sdougos, Sandy Williams, and Dick Fenner for their presence and moral support.

This research was supported by the National Science Foundation, Contract No.

TABLE OF CONTENTS

# NOMENCLATURE

## Filter properties

| | |
|---|---|
| $a$ | pore radius |
| h | thickness |
| P | porosity |
| $Z_f$ | sign of fixed charge |
| $\varepsilon_s$ | permittivity |
| $\rho_f$ | fixed charge density |
| $\sigma_s$ | conductivity |
| $\tau$ | tortuosity |

## Fluid properties

| | |
|---|---|
| $D_a$, $D_b$ | counterion and co-ion diffusivity |
| $t_a$ | transport number of counterion $(\kappa_a/\kappa_a+\kappa_b)$ |
| u | flow velocity |
| $\varepsilon_0$ | permittivity |
| $\kappa_a$,$\kappa_b$,$\kappa_{AV}$ | counterion, co-ion, and average mobility |
| $\rho$ | charge density |
| $\sigma_0$ | conductivity (neutral) |

## Other variables

| | |
|---|---|
| F | Faraday's constant |
| J | current flux |
| S | streamwise coordinate |
| & | charging emf |
| $\phi$ | potential |

# CHAPTER 1:

# INTRODUCTION

Electrostatic charging hazards have been a well-known problem in the petroleum fuel handling industry for some years.[1] Although various components in fuel handling systems each contribute to the charging problem, the major contribution comes from the filtration portions of such systems.[2] Huber and Sonin have developed a theory that describes the charging process in the filtration of hydrocarbon fuels.[3] They conducted experiments filtering heptane through Millipore filters, and the results they obtained agree with their theory.[4] However, heptane, although a convenient liquid for laboratory studies, is rarely used in situations that create a charging hazard. In practice, due to their low conductivity and high rate of filtration, jet fuels are usually the liquids that pose the greatest charging hazard.

Since the major constituent of most jet fuels is kerosine, and in an effort to relate the theory to more typical charging situations, we conducted experiments in which we filtered kerosine through Millipore filters and compared these experimental results with the theory. Some of the results of the experiments lie in a region where Huber and Sonin do not provide an explicit analytical solution. Nevertheless, the experimental results and the theory do agree outside this region and, as with the experimental results for heptane, rough values for the mobility of the ions in the working fluid are inferred.

Chapter 2 reviews the theory of Huber and Sonin, and a description of the apparatus, working fluid, and filters appears in Chapter 3. The comparison of the experimental results and the theory is given in Chapter 4.

# CHAPTER 2:

# THEORY

Whenever liquids and solids come into contact with each other, a charge migration occurs at the interface that results in the solid and liquid each attaining a net electric charge. A charge distribution develops in the liquid near the interface due to the balance between the electrostatic attraction of the charge in the fluid to the charge in the solid and the diffusion of this fluid charge away from the interface. This charge distribution can be characterized by its length, $\lambda_D$ , the Debye length, where

$$\lambda_D = \left(\frac{\epsilon_0 D_{AV}}{\sigma_0}\right)^{\frac{1}{2}} \quad . \tag{1}$$

$\epsilon_0$ is the permittivity of the fluid, $\sigma_0$ is the conductivity of the fluid, and $D_{AV}$ is the average diffusivity of the ions in the liquid. If fluid is now forced to flow past this interface, the charge may be convected downstream and a potential charging hazard is created.

In the theory of Huber and Sonin, the solid-liquid interface occurs between a filter and a fuel and the charge distribution at the interface develops within the pores of the filter. One of the assumptions made in the development of the theory is that the Debye length is greater than the pore radius $a$ :

$$\lambda_D > a \quad . \tag{2}$$

When $\lambda_D > a$ , the charge distribution in the pore is nearly uniform

and a bulk model for convection of charge in the fluid within the filter can be assumed. From Eq. (1) one can see that the assumption of "large" Debye length is equivalent to having a low fluid conductivity. This is consistent with the condition encountered in practical fuel filtration situations.

Also, to aid in the solving of the governing equations, a one-dimensional flow situation is assumed. That is, the filter is planar and the fluid flow and the current are normal to the filter. We can now write the constitutive relations. The current density in the fluid is

$$J = -Z_f \rho u - \sigma \frac{d\phi}{dS} + Z_f F \left( D_a \frac{dC_a}{dS} - D_b \frac{dC_b}{dS} \right) \quad , \qquad (3)$$

where the first, second, and third terms on the right hand side represent the convection, the conduction, and the diffusion of charge, respectively. If the current density is assumed to be small ($J \ll \rho u$), then this expression can be integrated to give the net charging emf across the filter,

$$-Z_f \mathscr{E} = \int_{-\infty}^{+\infty} \frac{d\phi}{dS} \, dS = \int_{-\infty}^{+\infty} \frac{\rho u}{\sigma} \, dS \quad . \qquad (4)$$

Notice that the diffusive term has disappeared. If electrodes are placed upstream and downstream of the filter, outside of the charge distribution, then the filter will appear to be a flow driven voltage source in series with the resistance of the fluid. In order to integrate Eq. (4), expressions for $\rho$, $u$, and $\sigma$ must be derived. Since

the geometry is one-dimensional, the flow velocity $u$ is a constant. The conductivity of the fluid as a function of the charge density in the fluid is

$$\sigma = \sigma_0 \left[ (1+\gamma^2)^{1/2} + (2t_a - 1)\gamma \right] , \qquad (5)$$

where $\sigma_0$ is the conductivity of the electrically neutral fluid ($\rho = 0$) and $\gamma$ is the dimensionless charge density in the fluid,

$$\gamma = \frac{\rho K_{AV}}{\sigma_0} . \qquad (6)$$

A differential equation for the charge density as a function of the stream coordinate is now derived by eliminating the potential gradient term from Eq. (3) using Poisson's equation:

$$\frac{d^2\phi}{dS^2} = \frac{Z_f \rho}{\varepsilon_0} . \qquad (7)$$

Using these expressions for $\rho$ and $\sigma$, Huber and Sonin completed the integration in Eq. (4) and the resulting solutions are governed by two dimensionless parameters. The first is the charge relaxation length divided by the filter thickness:

$$\theta = \frac{\varepsilon_0 u}{\sigma_0 h} . \qquad (8)$$

Here, $\varepsilon_0/\sigma_0$ is the relaxation time of charge in the fluid, $\varepsilon_0 u/\sigma_0$ is the charge relaxation length, and $\varepsilon_0 u/\sigma_0 h$ is the dimensionless charge relaxation length. The second parameter is the dimensionless filter fixed charge, $\gamma_f$ :

$$\gamma_f = \frac{\rho_f K_{AV}}{\sigma_0} . \qquad (9)$$

The low fixed charge solution, which applies when $\gamma_f << 1$ or $\gamma_f << \theta$ (see Fig. 1), is

$$-Z_f^{\&} = \rho_f \frac{\tau^2}{\sigma_0}\left(\frac{uh}{P}\right)\left\{1 - \left(1 - \frac{P^2}{T^2}\right)\frac{\varepsilon_f\theta}{\varepsilon_0 P^2}\left[1 - \exp\left(\frac{-\varepsilon_0 P^2}{\varepsilon_f\theta}\right)\right]\right\} \qquad (10)$$

where $\varepsilon_f = P\varepsilon_0 + (1-P)\varepsilon_s$ is the permittivity of the filter impregnated with fluid. For large and small values of $\theta$ this expression can be simplified to

$$-Z_f^{\&} = \rho_f \frac{\tau^2}{\sigma_0}\left(\frac{uh}{P}\right) \qquad \theta << 1 \qquad (11a)$$

$$-Z_f^{\&} = \rho_f \frac{P^2}{\sigma_0}\left(\frac{uh}{P}\right) \qquad \theta >> 1 \quad .$$

The high fixed charge solution, which applies when $\gamma_f >> 1$ and $\gamma_f >> \theta$ (again, see Fig. 1), is given by

$$-Z_f^{\&} = \frac{\tau^2}{\kappa_a}\left(\frac{uh}{P}\right)\left[1 + \frac{F(t_a)}{\tau^2}(\theta P)\right] \qquad (12)$$

where

$$F(t_a) = \frac{1}{4}\left[\frac{2t_a - 1}{t_a - 1} + \frac{1}{(1-t_a)^{3/2} t_a^{1/2}} \tan^{-1}\left(\frac{1-t_a}{t_a}\right)^{1/2}\right] .$$

For large and small values of $\theta$ this expression can also be simplified to

$$-Z_f\mathcal{E} = \frac{\tau^2}{\kappa_a}\left(\frac{uh}{P}\right) \qquad \theta << 1 \tag{13a}$$

$$-Z_f\mathcal{E} = \frac{F(t_a)}{\kappa_a}\left(\frac{uh}{P}\right)\theta P \qquad \theta >> 1 \quad . \tag{13b}$$

There are two things that should be noted in Eqs. (11) and (13). First, Eq. (13b) is parabolic in mean flow velocity ($\theta \propto u$), whereas the other expressions for charging emf are linear in flow velocity. Second, the low fixed charge solutions, Eq. (11), are linearly dependent on the filter fixed charge, a quantity that is generally unknown, whereas the high fixed charge solutions are independent of filter fixed charge. Both of the points will be discussed in greater detail in Chapter 4. In the following chapter we will describe the apparatus and the procedure used to experimentally investigate the theory.

# CHAPTER 3:

# APPARATUS

In order to test the theory, experiments were performed in which kerosine was passed through various Millipore filters. Electrodes upstream and downstream of the filter measured the charging emf's created by the flow through the filters so that these measured emf's could be compared with the theoretically predicted behavior. The apparatus used was essentially the same as the one used by Huber and Sonin to measure the charging emf's across Millipore filters with heptane as the working fluid. Two separate flow cells were used. Each one held the filter perpendicular to the incident flow, but one was used for low flow rate experiments and the other for high flow rate experiments. Both test cells were made of plexiglas and were held in place by a 1½" PVC pipe. PVC and plexiglas have electrical conductivities that are much lower than the electrical conductivity of the working fluid. A diagram of the low flow rate test cell appears in Fig. 2. In this test cell, the filters are edge-supported by sealing them against the PVC flange with an O-ring resulting in $1.02 \times 10^{-3}$ $m^2$ of filter area exposed to the oncoming flow. The high flow rate test cell appears in Fig. 3. In this test cell the filter is supported over most of its area and 61 parallel channels present a total area of $1.51 \times 10^{-4}$ $m^2$ to the oncoming flow.

Stainless steel tanks upstream and downstream from the test cell

provide reservoirs for the fluid. The upstream tank is pressurized with pre-purified nitrogen gas which forces the kerosine through flow gauges and nylon and PVC pipe to the test cell. Kerosine exiting the test cell is deposited in the downstream tank.

In both test cells stainless steel electrodes are situated upstream and downstream of the filter. The upstream electrode is grounded and either the potential difference across the electrodes or the current passing through the electrodes is measured by a Keithley 610B Electrometer. The electrodes are connected to the electrometer via about 30 feet of teflon-coated, shielded wire. The filter, fluid, electrodes, cables, and electrometer all form an electric circuit whose schematic appears in Fig. 4.

The filter emf, $\mathcal{E}$, is in series with the fluid resistance $R_0$, and the resulting voltage or current is measured by an external resistance, $R_e$. The fluid resistance is governed by the geometry of the test cell and the fluid conductivity. The resistance is

$$R_0 = \frac{\ell}{A\sigma_0} \quad , \tag{14}$$

where $\ell$ is the distance between the electrodes and $A$ is the cross-sectional area of the pipe. The charging emf can be related to the measured voltage or current by the following relationship:

$$\mathcal{E} = (R_0 + R_e)\frac{\Delta\phi}{R_e} = (R_0 + R_e)I \quad , \tag{15}$$

where $\Delta\phi$ and $I$ are the measured voltage and current, respectively. In instances where the measured voltage exceeded 100 volts, a Keithley

6103A 1000:1 voltage divider was used with $R_e = 4.5 \times 10^{11}\ \Omega$ ; otherwise, the external resistance, $R_e$ , was controlled by the electrometer.

As with the experiments of Huber and Sonin, we increased the conductivity of the working fluid kerosine by doping with Shell's antistatic additive, ASA-3. Figure 5 is a plot of the conductivity of both heptane and kerosine as a function of the concentrations of ASA-3. There were three reasons for the addition of the ASA-3. First, the conductivity of the kerosine received was only $4.1 \times 10^{-11}$ mhos/m. In order to easily measure the charging emf, the current should not be too small. Since the current is controlled by $R_0$ , we increased the fluid conductivity to about $3 \times 10^{-10}$ mhos/m. Second, as a by-product of matching the experimentally measured emf's to the theory, we can infer values of the mobility of the ions in the fluid. In order for this to be meaningful, the ions should be from a well-known, controlled additive. By increasing the conductivity of the kerosine an order of magnitude above its virgin conductivity, we ensure that the electrical properties of the fluid are controlled by the ASA-3. Third, airlines and governments that have jet fuel conductivity specifications usually require their fuel to have a conductivity between $0.5\text{-}3.0 \times 10^{-10}$ mhos/m.[5] Most potential charging hazards occur during the fueling of commercial or military aircraft when fuel is moved rapidly from a holding tank through a filter to the aircraft wing. Since these fuels are very pure, their conductivity is usually low and this, combined with the rapid rates at which the fuel is filtered, results in a very large charging relaxation

length ($\theta = \varepsilon_0 u/\sigma_0 h$) and, consequently, a large charging hazard.

The primary military jet fuels are the Airforce's JP-4 and the Navy's JP-5. The corresponding commercial jet fuels are Jet B and Jet A or A-1. JP-4 and Jet B are composed of heavy naphtha and kerosine blend, whereas JP-5 and Jet A and A-1 are composed primarily of kerosine.[6] If these jet fuels exhibit the behavior of their major constituent, then experiments with kerosine will be representative of experiments and the charging situation with real jet fuels.

Three kinds of Millipore filters were used in the experiments and their properties are summarized in Table 1. Each filter was handled carefully so that it would not become contaminated. Each one was initially soaked in the kerosine for at least 48 hours before testing and was then rapidly transferred to the test cell without being allowed to dry out.

The theory of Huber and Sonin only describes the steady-state charging emf created by the flow through the filter. There are time constants associated with the charging processes and the measuring apparatus that must be considered in order to meet actual steady-state conditions. When the flow velocity is altered in the apparatus a new charge distribution is created near the filter and therefore a new charging emf. The time constant of this change is on the order of the charge relaxation time in the fluid, $\varepsilon_0/\sigma$ , which in our case was on the order of 0.06 sec. The capacitive charging time of the filter is on the same order as this value. All dynamic processes that have time constants much greater than this can be described by the steady

state theory. The measuring portion of the apparatus also has a time constant associated with it; the voltage created by the filter is measured by the two electrodes that are attached to the electrometer through about 30 ft. of coaxial cable. At 50 pf/ft the total capacitance of the cable is about 1500 pf. This capacitance is charged through a fluid conductance on the order of $15 \times 10^{-12}$ mhos for the low flow rate apparatus and on the order of $2 \times 10^{-12}$ mhos for the high flow rate apparatus, resulting in time constants of 100 sec and 750 sec, respectively. Whenever a flow rate was altered, we waited a span of a few time constants before taking a reading.

Other precautions were taken during the measurement of the charging emf's. The walls of the pipes and tubes that connect the test cells to the reservoirs may also have a fixed charge and therefore a resulting charging emf current is created by them. These potentials were measured in the absence of a filter. We ensured that charging emf's measured with filters in place were much greater than these streaming potentials. Also, it was noted that on excessively humid days, the measured data fell significantly below the values found on other days. This data was naturally discarded. Since the kerosine does not come in contact with the atmosphere, we have assumed that the humidity effect is a result of the shorting out of the wires that lead from the electrodes to the electrometer through the highly conducting humid air. Finally, we were careful to keep the pressure in the starting tank low so that dissolved nitrogen would not alter the properties of the kerosine.

# CHAPTER 4:

# DATA

As pointed out earlier in the review of the theory, the solutions for the charging emf's obtained by Huber and Sonin are governed by the magnitude of two dimensionless parameters. The first is the dimensionless filter fixed charge density, $\gamma_f$ , where

$$\gamma_f = \frac{\rho_f \kappa_a}{\sigma_0}$$

and $\rho_f$ is the fixed charge in the filter per unit pore volume. The group $\sigma_0/\kappa_{AV}$ is the conductivity of the electrically neutral fluid divided by the average mobility of the ions in the fluid and from the definition of the conductivity of the electrically neutral fluid,

$$\sigma_0 = F\kappa_{AV}2C_0 \quad , \tag{16}$$

one can see that $2C_0$ represents the concentration of ions (both negative and positive) in the electrically neutral fluid. With the conductivity used in our experiments ($\sim 3\times10^{-10}$ mhos/m) and an estimate of the mobility of the ions ($\sim 3\times10^{-9}$ m$^2$/V-sec), the "charge density" in the neutral fluid in our experiments is estimated to be about 0.1 coul/m$^3$. This corresponds to about two singly-charged ions per million molecules in the fluid, a very low concentration.

The second parameter is the dimensionless charge relaxation length, $\theta$ , where

$$\theta = \frac{\varepsilon_0 u}{\sigma_0 h} \quad .$$

$\varepsilon_0/\sigma_0$ is the relaxation time of charge in the fluid and $\varepsilon_0 u/\sigma_0$ is the convective charge relaxation length. Thus, $\theta$ is the ratio of the convection charge relaxation length to the filter thickness.

As mentioned earlier, the magnitude of these two parameters governs which solution for the charging emf applies. When $\gamma_f >> 1$ and $\gamma_f >> \theta$, then the solution lies in the high fixed charge regime; when $\gamma_f << 1$ or $\gamma_f << \theta$, then the solution lies in the low fixed charge regime. When $\gamma_f$ is between these two limits then there is no explicit analytic solution available, except when $\theta << 1$. An illustration of these regimes appears in Fig. 1. The solution for the charging emf in the high fixed charge regime is Eq. (12). Notice that when $\theta$ is small, this expression is linear in flow velocity, u, but as $\theta$ becomes large, the second term in the bracket begins to dominate and the charging emf begins to vary as the square of the flow velocity. The solution for the charging emf when the dimensionless filter fixed cahrge is small is given by Eqs. (11a) and (11b). Notice that for both large and small $\theta$, the dependence of charging emf on flow velocity and filter fixed charge is linear.

We found, for experiments where kerosine was being filtered by Millipore filters, that the measured charging emf's often appeared to fall in this low fixed charge regime. The filter fixed charge for $\gamma_f$ equal to, say 0.1, which we can consider to be in the low fixed charge regime, corresponds in our experiments to only about one fundamental charge per $10^{10}$ Å$^2$ of filter-filtrate interface, or about one electronic

charge per $10^{10}$ exposed filter atoms. Since this is such a sparse density, measured charging emf's in the low fixed charge regime, where the emf is expected to be linearly dependent on fixed charge, will be erratic and drift due to changes in fixed charge. These changes in fixed charge may be due to minute unknown and uncontrollable impurities in the fluid or chemical reactions between the filter and the fluid. In the high fixed charge regime, where the charging emf no longer depends on fixed charge, the measured emf's should be steady since even if the fixed charge changed the charging emf will remain unaffected.

As a result of the dependence of charging emf on the generally unknown fixed charge when $\gamma_f$ is small combined with the fact that the fixed charge density is a largely uncontrolled quantity, experimental confirmation of the theoretical dependence of charging emf on porosity P and thickness h is impossible in this limit. In order to experimentally confirm the dependence of charging emf on porosity and thickness, different filters must be used and they each may have completely different charge densities. It was impossible to distinguish between changes in fixed charge and changes in other filter parameters in our tests since we had no method of independently measuring the fixed charge. On the other hand, if the fixed charge is controlled by impurities, then the time scale of changes in fixed charge may often be much longer than the RC time constant of the measuring device and the dependence of charging emf on flow velocity can then be experimentally confirmed.

The magnitude of the parameter $\theta$ is easy to vary due to its

linear dependence on flow velocity. Therefore, let us consider how the charging emf depends on the filtration properties in the limits $\theta \ll 1$ and $\theta \gg 1$. First let us examine the limit $\theta \ll 1$. The results of the theory of Huber and Sonin are the expressions (11a) and (13a) for the charging emf when $\theta \ll 1$ .

In order to test the theory in the region $\theta \ll 1$ three kinds of Millipore filters were used: RA, EA, and NR grade. Some of the measured charging emf's for RA filters appear in Figs. 6, 7, and 8. Figure 6 shows the charging emf, $\mathcal{E}$ , plotted against $uh/P$ for one of the RA filters, RA3. The lines illustrate the linear dependence of charging emf on flow velocity at three different times. The other RA filters showed a similar behavior. The number of point that show a linear dependence of charging emf on flow velocity is small because uncontrolled, continual changes in fixed charges did not allow long test times at any given fixed charge. Due to time constants in the measuring apparatus, it took about an hour to trace out a plot of charging emf versus flow velocity. A linear relation was usually obtained, indicating that the changes in fixed charge were small during that hour. At times, however, the relation was nonlinear, from which one might assume that the fixed charge had changed. For large fixed charge, however, the linear relation is more readily observed since the charging emf no longer depends on fixed charge and $\mathcal{E}P/uh$ remains constant.

In Fig. 7 the slope, $\mathcal{E}P/uh$, is plotted versus the time that each filter was exposed to flow conditions (the flow hours, t) for five

different RA filters. The theory states that when $\theta \ll 1$ ,

$$-Z_f \frac{\&P}{uh} = 2 \frac{\tau^2}{\kappa_a} \frac{\gamma_f t_a}{f(\gamma_f)} \quad , \tag{17}$$

where $f(\gamma_f) = (1+\gamma_f^2)^{1/2} + (2t_a - 1)\gamma_f$ . The behavior of this expression is illustrated in Fig. 8. Notice that when $Z_f\gamma_f$ becomes large (either positive or negative), then $\&P/uh$ reaches an asymptote whose intercept value is $\tau^2/\kappa_a$ and no longer depends on $\gamma_f$ .

Clearly, if $\gamma_f \ll 1$ , the parameter $\&P/uh$ may vary with time and be different for each RA filter if $\gamma_f$ is different for each (as may be the case if the fixed charge is affected by uncontrolled impurities). But if $\gamma_f \gg 1$ , $\&P/uh$ should be the same for each filter and time invariant because $\tau^2/\kappa_a$ is the same for each filter and a constant in time.

All of the RA filters represented in Fig. 7 begin with a positive voltage; then after about 6 hours of flow, the voltage changes to negative, and finally after about 10 hours, the value of $\&P/uh$ becomes a constant. This can be interpreted in terms of the theory as follows. The fixed charge starts at some initial negative value ($\& > 0$), and as the filter flows through the filter, the fixed charge drifts towards zero and eventually changes to positive ($\& < 0$). Upon further exposure to the flow, the fixed charge continues to increase until $\gamma_f$ becomes much greater than one and $\&P/uh$ assumes a constant value.

Qualitatively the theory of Huber and Sonin and the measured behavior

agree, but they also agree quantitatively. First, in Fig. 7 the values of $\Delta P/uh$ observed after about 10 hours of flow are the same within the uncertainty in P, h, and $\tau$ from one filter to the next, and are much steadier than values of $\Delta P/uh$ observed before 6 hours of flow. This is consistent with the high fixed charge solution where $\Delta P/uh$ is independent of $\rho_f$ .

Second, if we assume that the high fixed charge limit has been reached, a value for the mobility of the negative ASA-3 ion in kerosine can be inferred. Three of the filters reach asymptotes that are relatively close together, RA #2, #3, and #4, whereas RA #1 reached an asymptote at a higher value of $\Delta P/uh$ . It would seem that the higher value in the case of RA #1 is probably due to one or more of the properties of this filter being atypical of RA filters (smaller porosity, larger thickness, etc.) and that the mobility can be inferred from the value of $\Delta P/uh$ observed in RA #2, #3, and #4, assuming $\tau_{RA} \sim 1$:

$$\kappa_- \simeq 0.8 \times 10^{-8} \text{ m}^2/\text{V-sec} \quad .$$

This is a physically reasonable value.[8]

We have shown how the measured emf's and the theory agree for inferred values of the mobility, $\kappa_-$ , and the dimensionless filter fixed charge.

Figure 9 shows the charging emf $\mathcal{E}$ versus $uh/P$ for three separate RA filter thicknesses, 150 μm, 450 μm, and 750 μm, obtained by sandwiching several filters together. Although the fixed charge is

presumably different for each set of filters and for one set transient, the linear dependence on $u$ is still illustrated. The highest positive ratio of $\Delta P/uh$ found here is about $4.5 \times 10^8$ V-sec/m$^2$ and coincides well with the maximum value found in Fig. 7. Assuming this represents the high (negative) fixed charge case, we can, from these observations, estimate the mobility of the positive ASA-3 ion in kerosine to be

$$\kappa_+ = 0.2 \times 10^{-8} \text{ m}^2/\text{V-sec}$$

for $\tau_{RA} \sim 1$. This value is physically reasonable and as with heptane, the mobility of the negative ASA-3 ion is greater than the mobility of the positive ASA-3 ion.

Similar experiments were performed with EA and NR filters and the measured charging emf's appear in Figs. 10-14. Although the transition to high fixed charge was apparently not observed in any of these experiments, other facets of the theory can be illustrated. The linear dependence of charging emf on flow rate for various EA and NR filter thicknesses is illustrated in Figs. 11, 13, and 14 and the drift of the quantity $\Delta P/uh$ is shown for various thicknesses of EA filters in Figs. 10 and 12. In Fig. 10, the largest negative value observed for $\Delta P/uh$ is about twice the value seen for RA filters, which can be interpreted to indicate that the tortuosity of the EA filter is about 1.5 times larger than the tortuosity of the RA filter. This compares well with the ratio of the tortuosities found by Huber and Sonin in their experiments with heptane.

We have shown how the experimentally measured charging emf for kerosine flowing through TA, EA, and NR Millipore filters agree with the theory of Huber and Sonin for $\theta << 1$. We have described how they agree qualitatively and quantitatively, and we have also shown the linear dependence of charging emf on flow velocity. We also performed experiments where the value of the dimensionless charge relaxation length, $\theta$, was no longer much less than unity. The comparison of these experiments with the theory follows.

The theory of Huber and Sonin gives expressions for the charging emf across the filter in Eqs. (11b) and(12) when $\theta >> 1$. Notice that for high fixed charge, the dependence of charging emf on flow velocity changes from linear to parabolic as $\theta$ becomes large but when the fixed charge is low the dependence remains linear. To test the theory when the dimensionless charge relaxation length $\theta$ is no longer small, Millipore RA and EA filters were employed in the high flow rate apparatus. Figures 15, 17, and 18 represent the measured emf's for RA filters and Fig. 19 represents the measured emf's for EA filters. In Figs. 15, 17, and 18, the quantity $\&P/uh$ is plotted versus $\theta P$. Rearranging Eq. (12),

$$\frac{\&P}{uh} = \frac{\tau^2}{\kappa_a} + \frac{\tau^2}{\kappa_a}\frac{F(t_a)}{\tau^2}(\theta P) \quad . \tag{18}$$

We see that for $\gamma_f >> 1$ a straight line through the data in Figs. 15, 17, and 18 will intersect the vertical axis at $\tau^2/\kappa_a$ and have a slope $(\tau^2/\kappa_a)[F(t_a)/\tau^2]$. If the data is in the low fixed charge

regime, then the line will have slope zero and the intercept at $\theta = 0$ from the $\theta >> 1$ region will be

$$\frac{\&P}{uh} = \frac{P^2 \rho_f}{\sigma_0} \quad . \tag{19}$$

Therefore, one way to distinguish between a low fixed charge and a high fixed charge in the filter is by noticing the slope of the line drawn through the data. Figure 15 shows some measured charging emf's plotted in the way we have described. The point fall nicely on the line and we may conclude from this the following: First, we may conclude that the experiments agree with the theoretical dependence on velocity for $\gamma_f >> \theta$ and $\theta >> 1$ . Second, since the slope is not zero, the fixed charge is high in this particular experiment. Third, from the intercept we may infer a value for $\tau_{RA}^2/\kappa_-$ of $1.27 \times 10^8$ V-sec/m$^2$, a value that agrees well with the value found in Fig. 7 for $\theta << 1$ . Fourth, from the slope and this value of $\tau^2/\kappa_-$ , we find that $F(t_a)/\tau_{RA}^2 = 0.6$ . We note that data taken in earlier experiments did not always fit a straight line. Some results of such data appear in Figs. 17 and 18. In order to explain this data in terms of the theory, let us return to Fig. 1.

When $\theta$ is small, the line drawn through the points in both Figs. 17 and 18 has a non-zero slope. Let us assume that this is at point A' in Fig. 1. Point A' is determined by $\theta << \gamma_f$ and $\gamma_f >> 1$ . As the flow velocity increases, $\theta$ becomes larger and we move to point B'. At point B' we are in transition between the high and low fixed charge

solution and the value of $\theta$ found here is on the order of the value of $\gamma_f$ for the experiment. As $\theta$ increases further to C', we have left the high fixed charge regime and the parabolic dependence has given way to a linear one.

Figure 16 shows how the predicted behavior should appear and the information that can be inferred from the data. If $\gamma_f > 1$ but $\theta < \gamma_f$, then we should observe the behavior near point A in Fig. 18 which corresponds to point A' in Fig. 1. This line has a slope y and intercept x. As the velocity is increased, $\theta$ increases and we enter the transition region, B'. Upon further increases in $\theta$, we enter the low fixed charge regime and the behavior near point C' should be observed. The slope is zero and the intercept is z. From Eqs. (17) and (18) above we see that

$$x = \frac{\tau^2}{\kappa_a} \tag{20a}$$

$$y = \frac{\tau^2}{\kappa_a} \frac{F(t_a)}{\tau^2} \tag{20b}$$

$$z = \frac{P^2 \rho_f}{\sigma_0} \quad . \tag{20c}$$

In the experiments we performed, the value of $\gamma_f$ was found (by identifying experiment with theory) to be on the order of unity and the actual span of $\theta$ tested in the experiments is represented by points A, B, and C in Fig. 1. Figures 17 and 18 also show the location of these points since the behavior observed in Figs. 17 and 18 is similar to the behavior predicted in Fig. 1; even though the

constraint $\gamma_f >> 1$ has been been released, we can extrapolate the behavior expected in Fig. 16 into this region. The values of x, y, z, and $\theta_{trans}$ observed in Figs. 17 and 18 are summarized in Table 2, as are the values of $\gamma_f$, $\tau^2/\kappa_{AV}$, and $F(t_a)/\tau^2$ calculated from these observations. Notice that for both figures the values of $\theta_{trans}$ and $\gamma_f$ agree and that, within the scatter of the data, values of $\tau_{RA}^2/\kappa_-$ and $F(t_a)/\tau_{RA}^2$ compare between all three curves.

Experiments were also performed on EA filters in the high flow rate apparatus. The data appears in Fig. 19 where $\Delta P/uh$ has been plotted versus $\theta P$ as it has for the RA data. Notice that the fixed charge observed in these high flow rate experiments with EA filters was opposite to the fixed charge observed during the low flow rate experiments. We attribute this to the impurities in the fluid. The charge relaxation length $\theta$ varies between about 0.4 and 5.0 in the experiments. There seems to be conflicting evidence on the issue of whether or not the low charge solution applies here. On the one hand, the value of $\Delta P/uh$ does not decrease significantly for small $\theta$ and in fact a straight horizontal line fits the data well. This would support a low fixed charge assumption for this experiment. On the other hand, though, from the intercept value of $\Delta P/uh$ we find that $\gamma_f \cong 1.5$, definitely not within the low fixed charge regime. This discrepancy can be explained as follows. From the low charge relaxation length data we found that $\tau_{RA}^2/\kappa_+ \simeq 4 \times 10^8$ V-sec/m$^2$ and $\tau_{EA}/\tau_{RA} \simeq 1.5$. Combining, we can find an approximate value for the intercept

that we would observe in Fig. 17 if the fixed charge was very large.

$$\left(\frac{\&P}{uh}\right)_{inter.} = \frac{\tau_{EA}^2}{\kappa_+} = 9 \times 10^8 \text{ V-sec/m}^2 \quad .$$

This is more than a factor of 4 higher than the intercept value observed.

We do expect that the low $\theta$ behavior observed in Figs. 14, 15, and 16 for RA filters will appear until the values of $\&P/uh$ measured approach or exceed $\tau^2/\kappa_a$ . In this case they clearly do not and as a result this seems to be one of the cases where neither the low nor high fixed charge solutions can be applied with confidence.

We have shown how the measured charging emf's from Millipore RA and EA filters compare with the theory of Huber and Sonin when the dimensionless charge relaxation $\theta$ is no longer much less than unity. We have shown that the RA filter data matches the theory in the high fixed charge limit and although there is no explicit analytical solution available for the charging emf when $\gamma_f$ is about one, the measured emf's for RA filters agree with the expected smooth transition between the high and low fixed charge solutions. And, in general, the dependence of measured charging emf on the various parameters investigated appears to agree with the theoretically predicted behavior when $\theta \geq 1$ .

From the value of $F(t_-)/\tau_{RA}^2$ found in Fig. 15, and for the values of the mobilities inferred from the low flow rate data, we can solve for the tortuosity of the RA filter, $\tau_{RA} \simeq 1.2$ . This is a physically

reasonable value and relatively close to the value found by Huber and Sonin in their experiments with heptane of 0.95 ± .11 .

# CHAPTER 5:

# CONCLUSIONS

We have examined the measured charging emf's is the limit $\theta << 1$ and when $\theta$ is no longer much less than unity. We have compared these measured emf's with the theory of Huber and Sonin and have shown that, insofar as a quantitative comparison is possible, the observed behavior agrees with the predicted behavior. The tortuosities of the filters and the mobilities of the ASA-3 ions in kerosine inferred from the data are physically reasonable values and the tortuosities we inferred show the same trends as the tortuosities inferred by Huber and Sonin for experiments with heptane.

The values for the inferred mobilities agree with values found using other techniques. For instance, Douwes and van der Waarden find the mobility of a Cr-DIPS ion in a gasoline fraction to be $0.32 \times 10^{-8}$ m$^2$/V-sec.[8] Considering the scatter of the data and general uncertainty in ion mobilities, we have come very close to the values found by others with our value of $\kappa_{AV} = 0.5 \times 10^{-8}$ m$^2$/V-sec.

In most of our experiments the observed behavior could be brought into agreement with the theory by assuming $\gamma_f \lesssim 1$ and, in general, the dimensionless fixed charge may often be small for practical fuel filtration situations. In experiments with heptane, Huber and Sonin found that a high fixed charge assumption applied when Millipore filters were used. But even so, in Huber and Sonin's experiments with Velcon filters, the fixed charge was found to be low and consequently

the same wide scatter and time variability of the charging emf was observed. Since it is reasonable that the charge density in the fluid is about the same as the charge density in the filter ($\gamma_f \sim 1$), the charging emf will usually depend on the unknown and uncontrollable fixed charge. Only when $\gamma_f >> 1$ and $\gamma_f >> \theta$ is the charging emf independent of fixed charge, and when the flow velocity is large ($\theta >> 1$), as is usually the case in practical fuel handling situations, the fixed charge is even less likely to fall in the high fixed charge regime.

For these reasons, we would suggest that the charging problem in many cases is determined not only by the fluid mechanics but equally by the chemistry of the filter-fluid interface. A better understanding of the fixed charge, a property controlled by the chemistry of the filter-fluid interface, is necessary if a more complete understanding of the charging problem in filtration is to be attained.

# BIBLIOGRAPHY

1. Klinkenberg, A. and van der Minne, J.L. (eds.), Electrostatics in the Petroleum Industry, Elsevier, Amsterdam, 1958.
2. Leonard, J.T., "Principles of Electrostatics in Aircraft Fuel Systems," 1972 Lightning and Static Electricity Conference, AFAL-TR-72-325.
3. Huber, P.W. and Sonin, A.A., J. Coll. Interface Sci., 61, 109 (1977).
4. Huber, P.W. and Sonin, A.A., J. Coll. Interface Sci., 61, 126 (1977).
5. "Jet Fuel Specifications," Esso Research and Engineering Co. (1973).
6. Dukek, W.C., in Encyclopedia of Science and Technology, Vol. 7, McGraw Hill, 1977, p. 340.
7. "1976 Millipore Catalogue and Purchasing Guide," Millipore Co., Bedford, Mass., No. MC 176/P (1976).
8. Douwes, C. and van der Waarden, M., J. Inst. Petr., 53, 237 (1967).

TABLE 1. Filter Properties

| Filter Type | CATALOG DATA[7] | | | |
|---|---|---|---|---|
| | Material | Thickness (μm) | Porosity | Pore radius (μm) |
| RA | mixed cellulose esters | 150 | 0.82 | 0.6 |
| EA | cellulose acetate | 130 | 0.74 | 0.5 |
| NR | nylon | 150 | 0.63 | 0.5 |

TABLE 2. Summary of Data for RA Filters when $\theta > 1$

| Figure | x | y | z | $\theta_{trans}$ | $\gamma_f$ | $\tau^2/\kappa_-$ | $\frac{F(t_-)}{\tau^2}$ |
|---|---|---|---|---|---|---|---|
| | ($10^8$ V-sec/m$^2$) | | | | | $10^8 \frac{\text{V-sec}}{\text{m}^2}$ | |
| 9 | 1.27 | 0.71 | - | - | - | 1.27 | 0.56 |
| 10 | 1.01 | 0.65 | 1.98 | 1.5 | 1.47 | 1.01 | 0.64 |
| 11 | 0.96 | 0.81 | 1.86 | 1.1 | 1.38 | 0.96 | 0.84 |

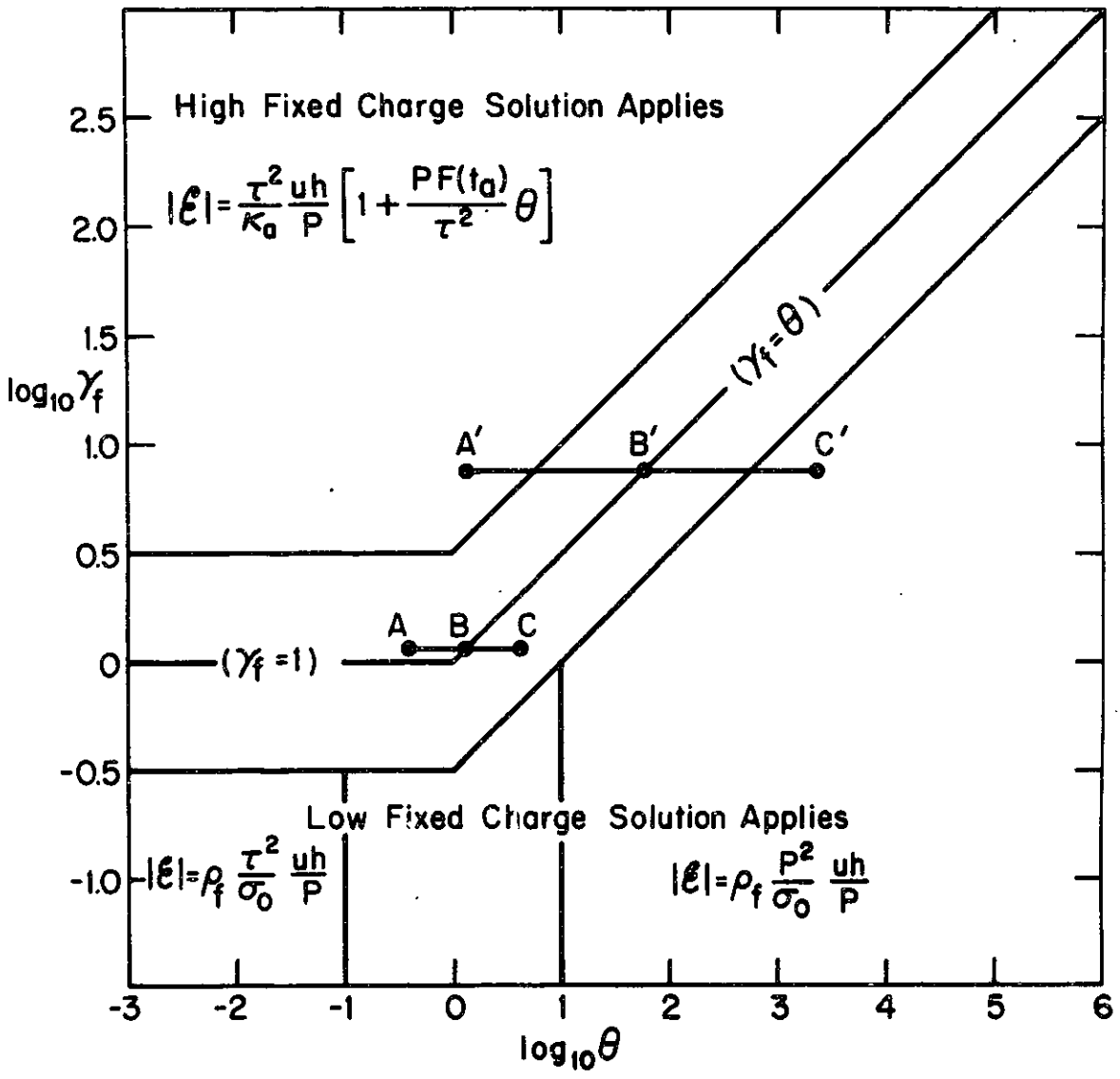


FIGURE 1. Operating conditions where low and high charge density solutions apply.

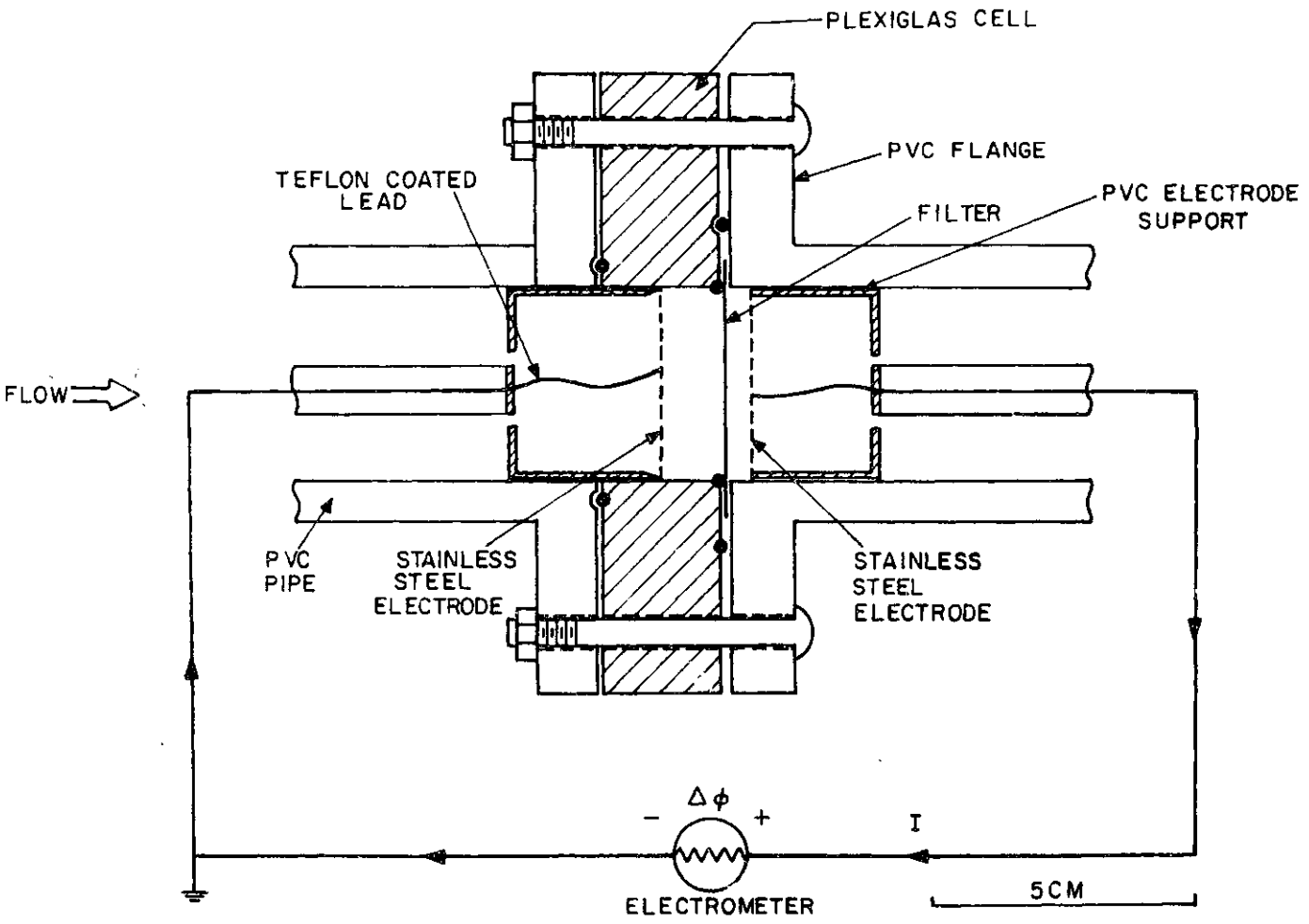


FIGURE 2. Low flow rate test cell.

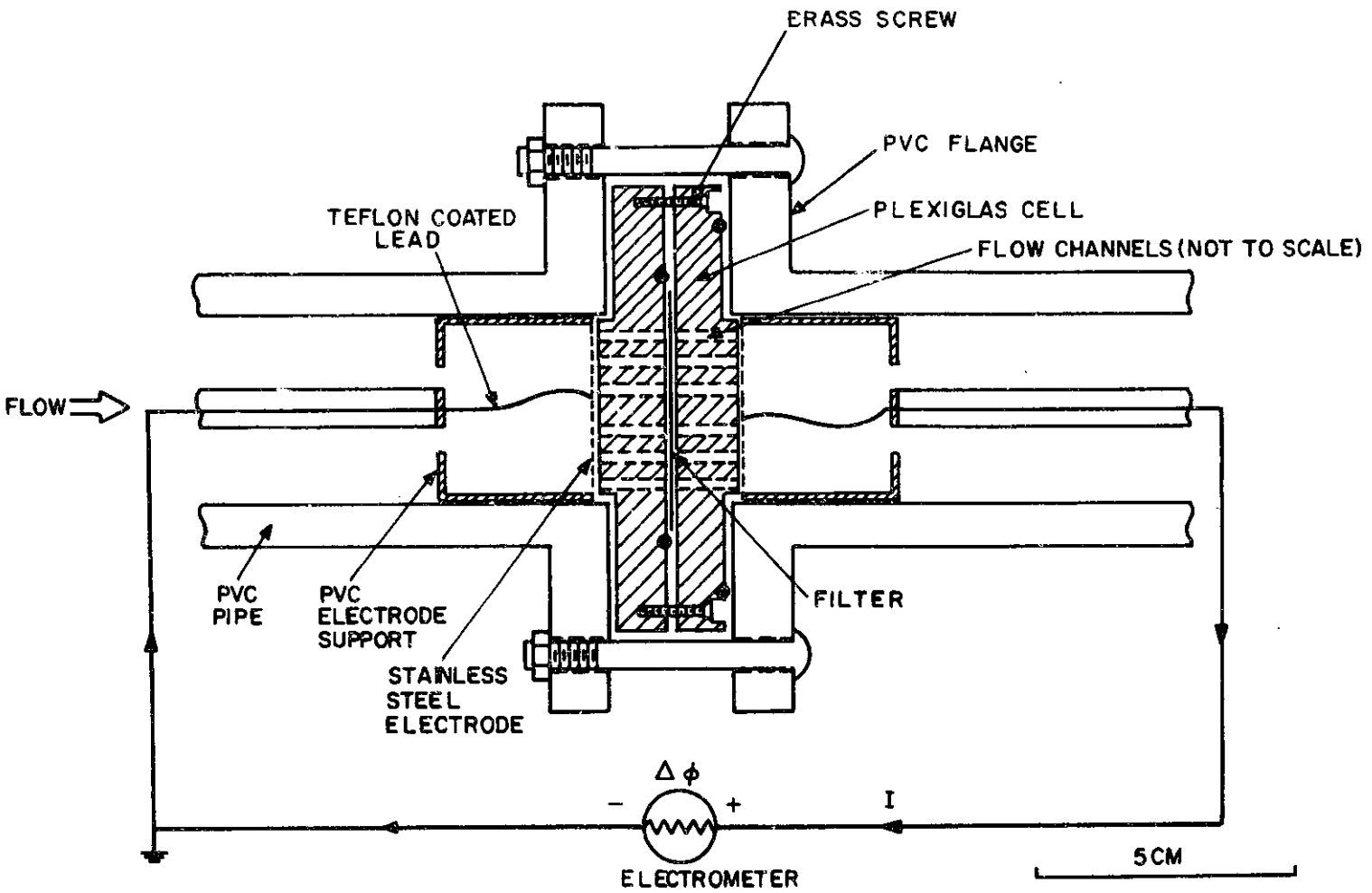


FIGURE 3. High flow rate test cell.

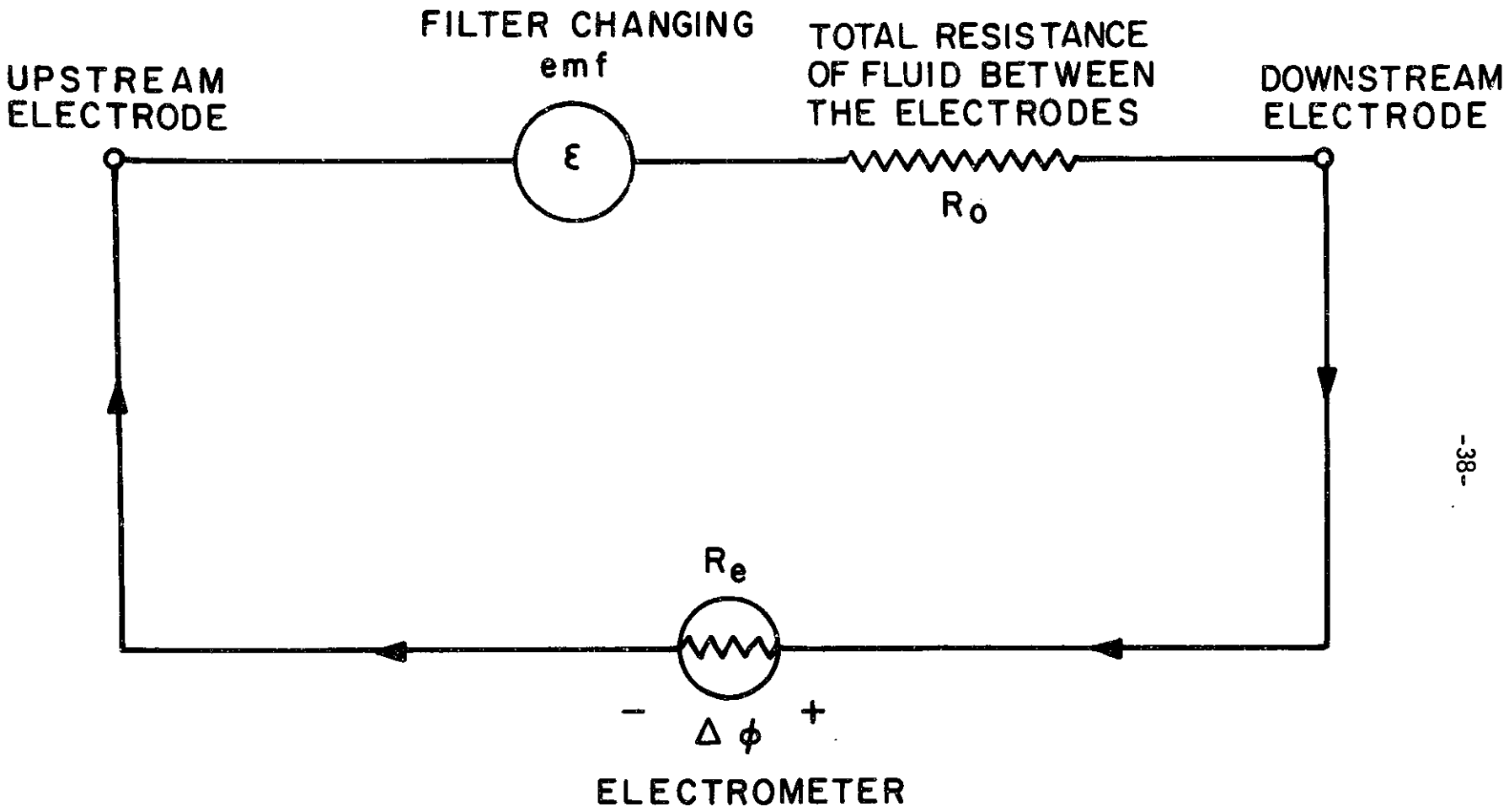


FIGURE 4. Schematic of filter-fluid-electrometer electric circuit.

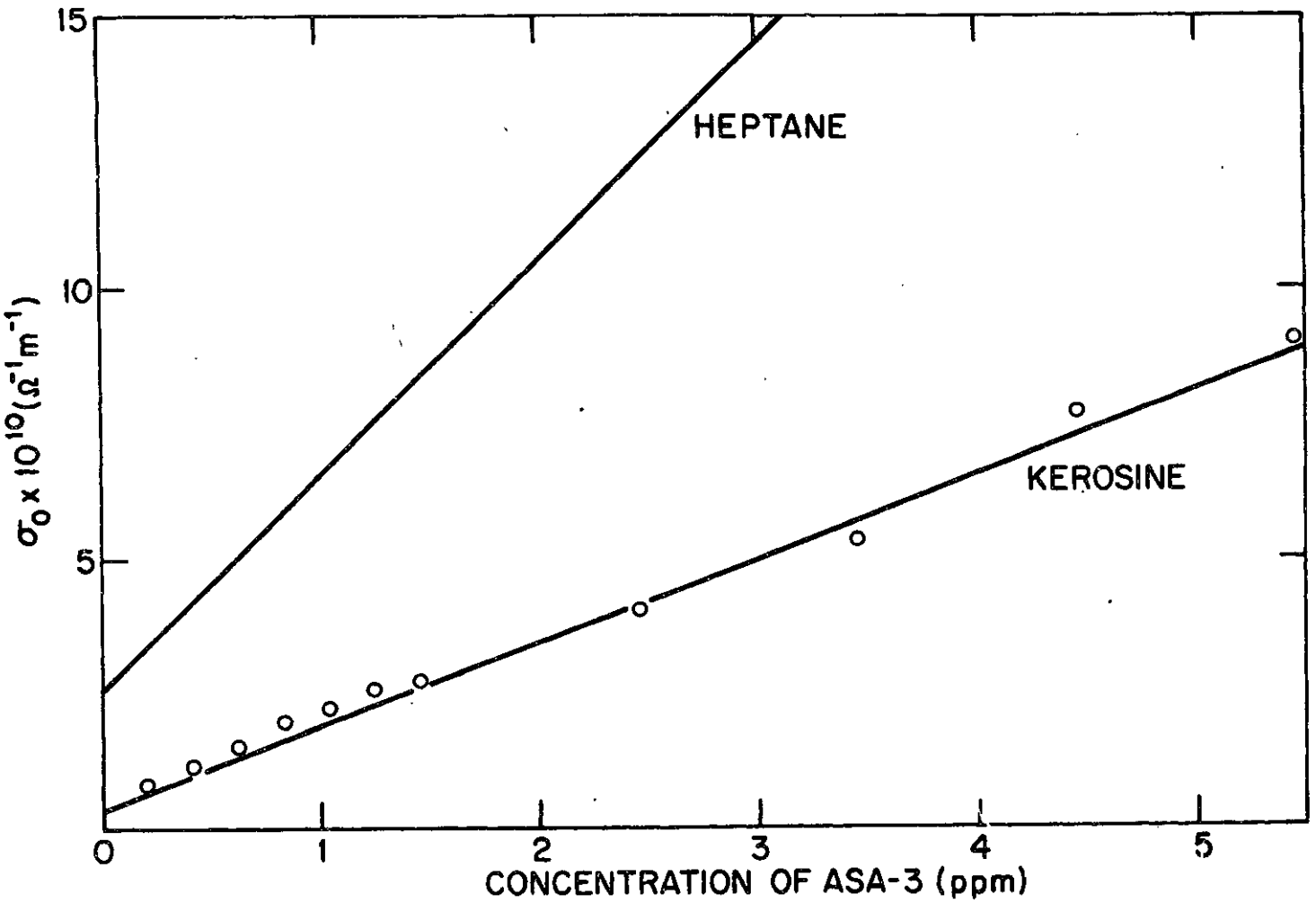


FIGURE 5. Conductivity of heptane and kerosine as a function of concentration of ASA-3.

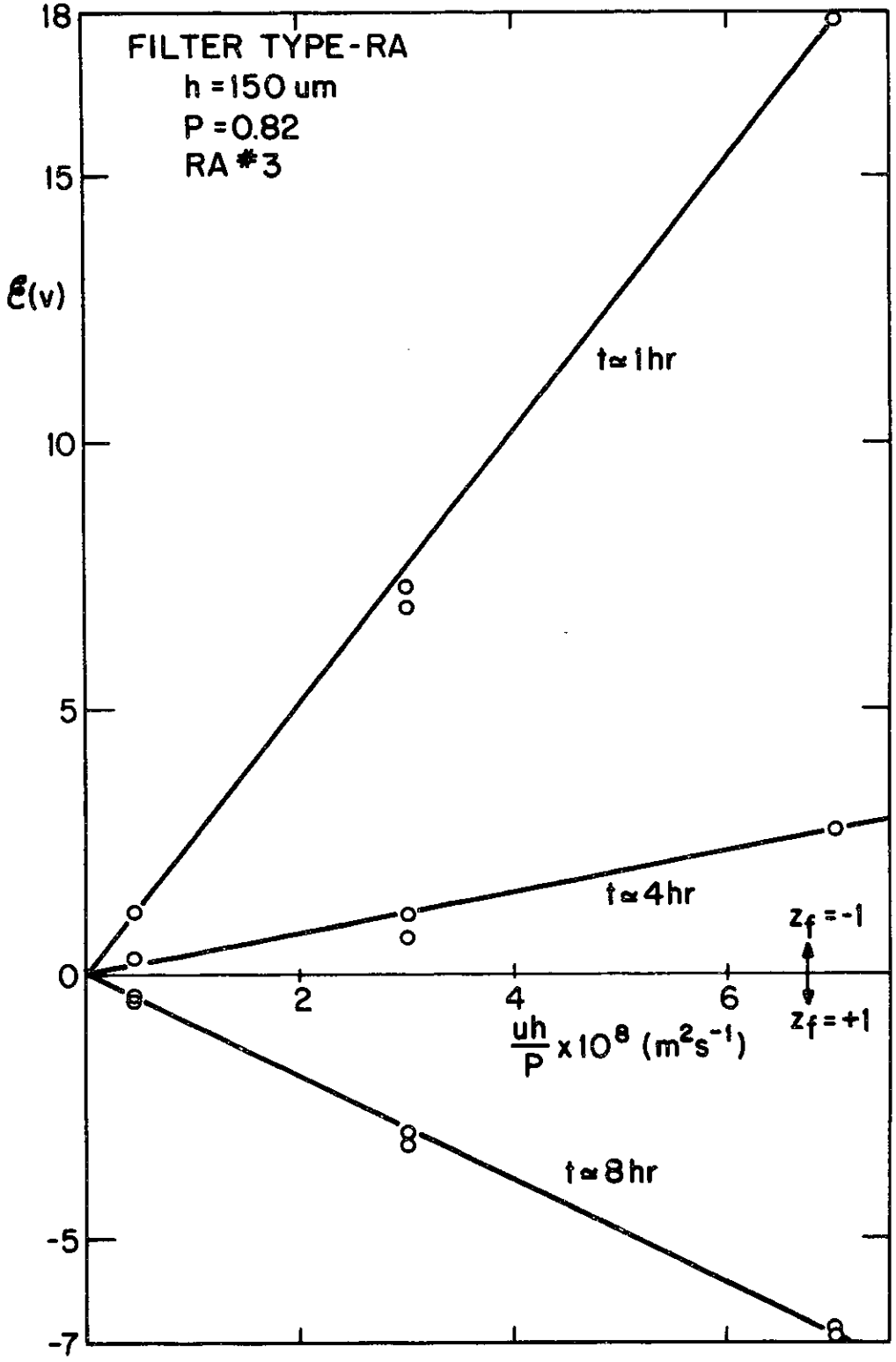


FIGURE 6. Charging emf as a function of reduced flow velocity for an RA filter, $\theta << 1$.

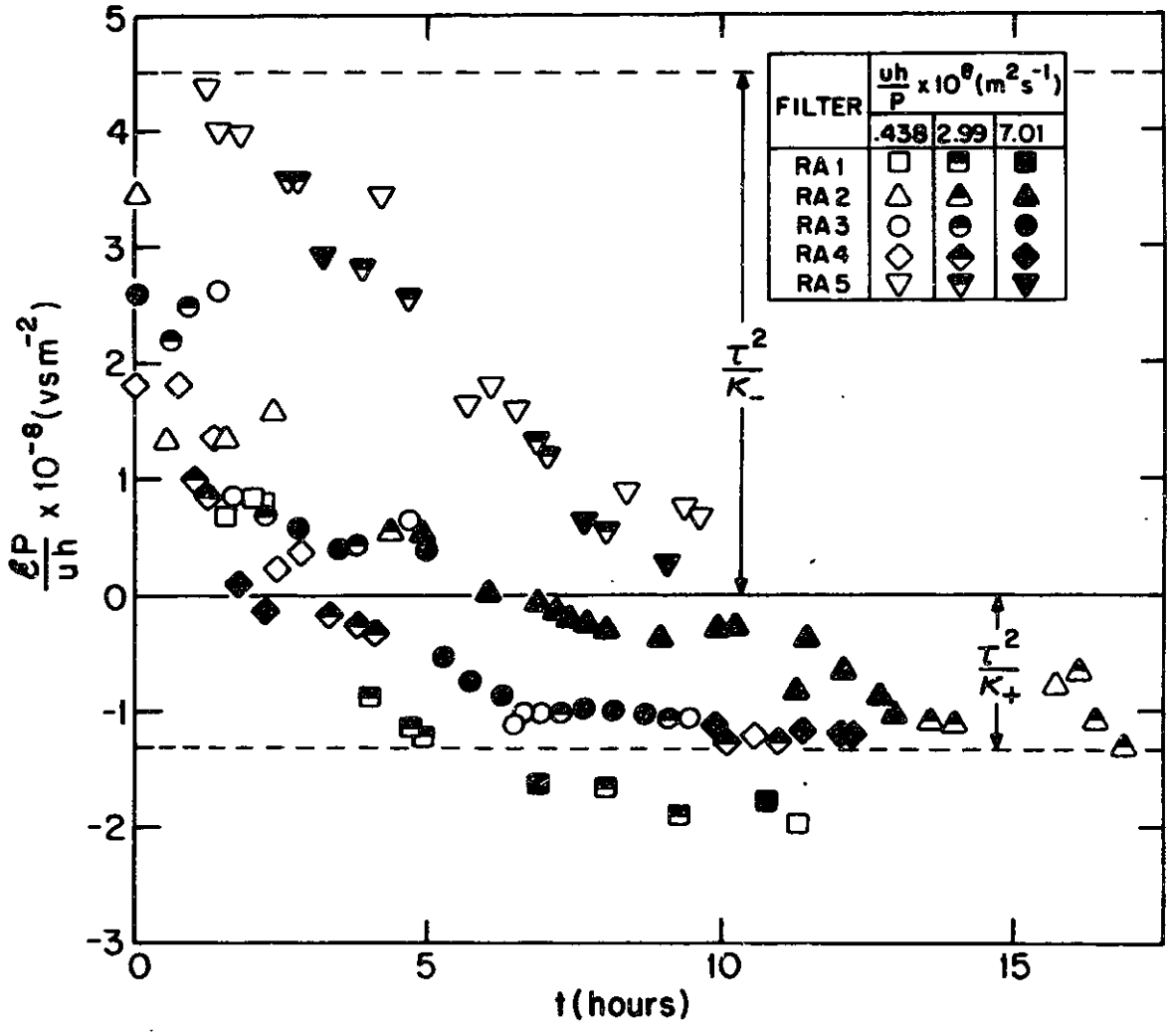


FIGURE 7. Reduced charging emf as a function of hours exposed to flow conditions for RA filters, $\theta \ll 1$.

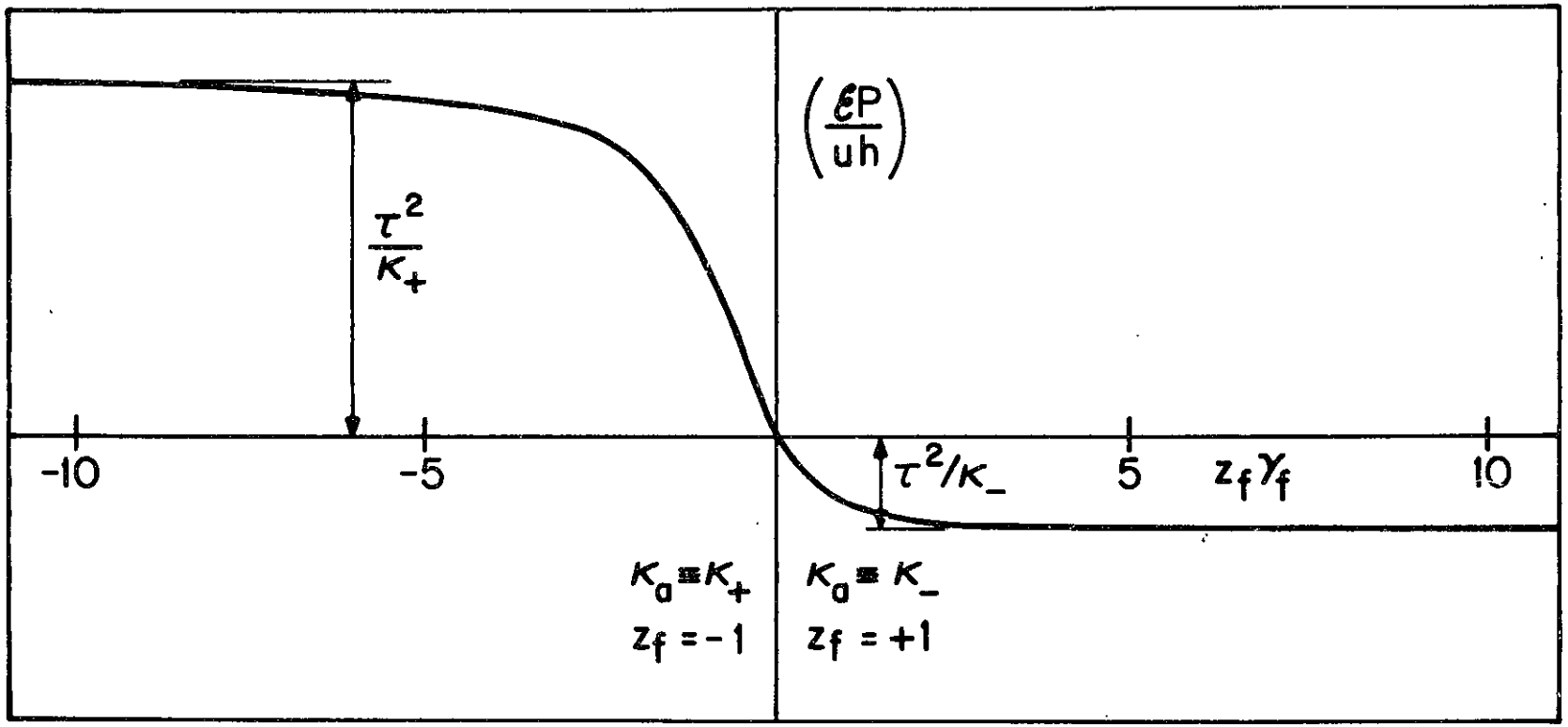


FIGURE 8. Theoretically predicted dependence of &P/uh on $\gamma_f$ for $t_+ = 0.2$, $t_- = 0.8$, and $\theta \ll 1$.

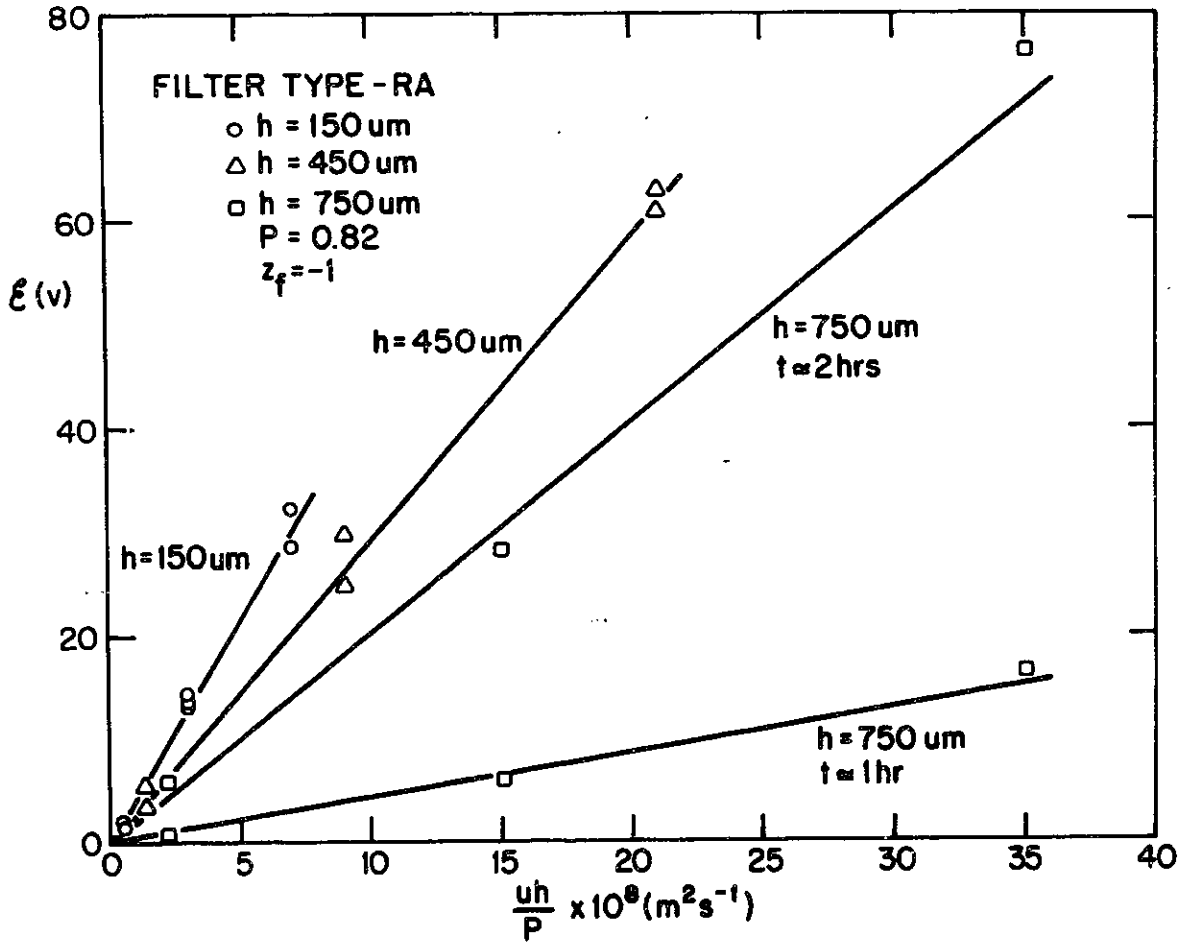


FIGURE 9. Charging emf as a function of reduced flow velocity for various RA filter thicknesses, $\theta \ll 1$.

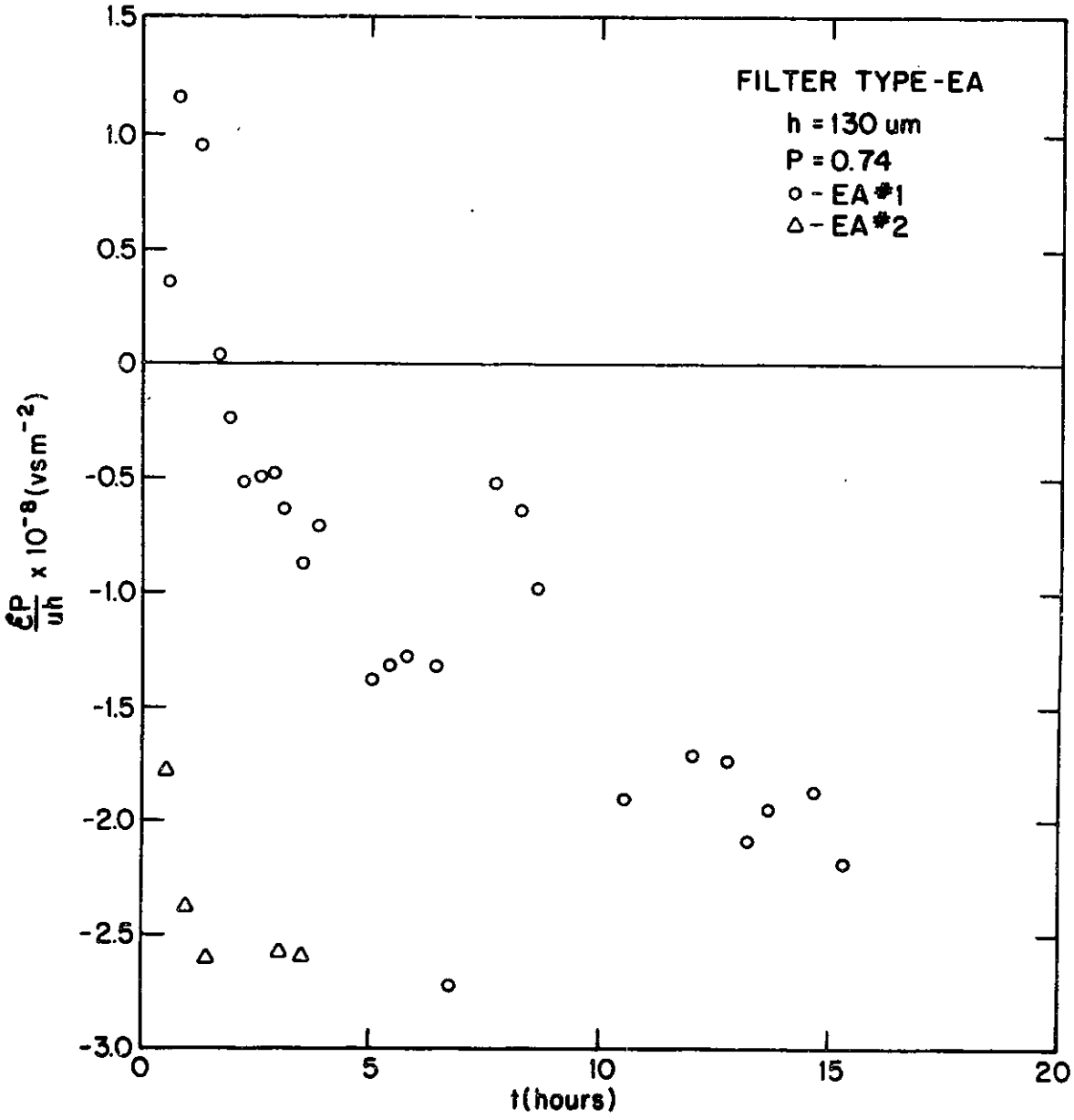


FIGURE 10. Reduced charging emf as a function of hours exposed to flow conditions for EA filters, $\theta << 1$.

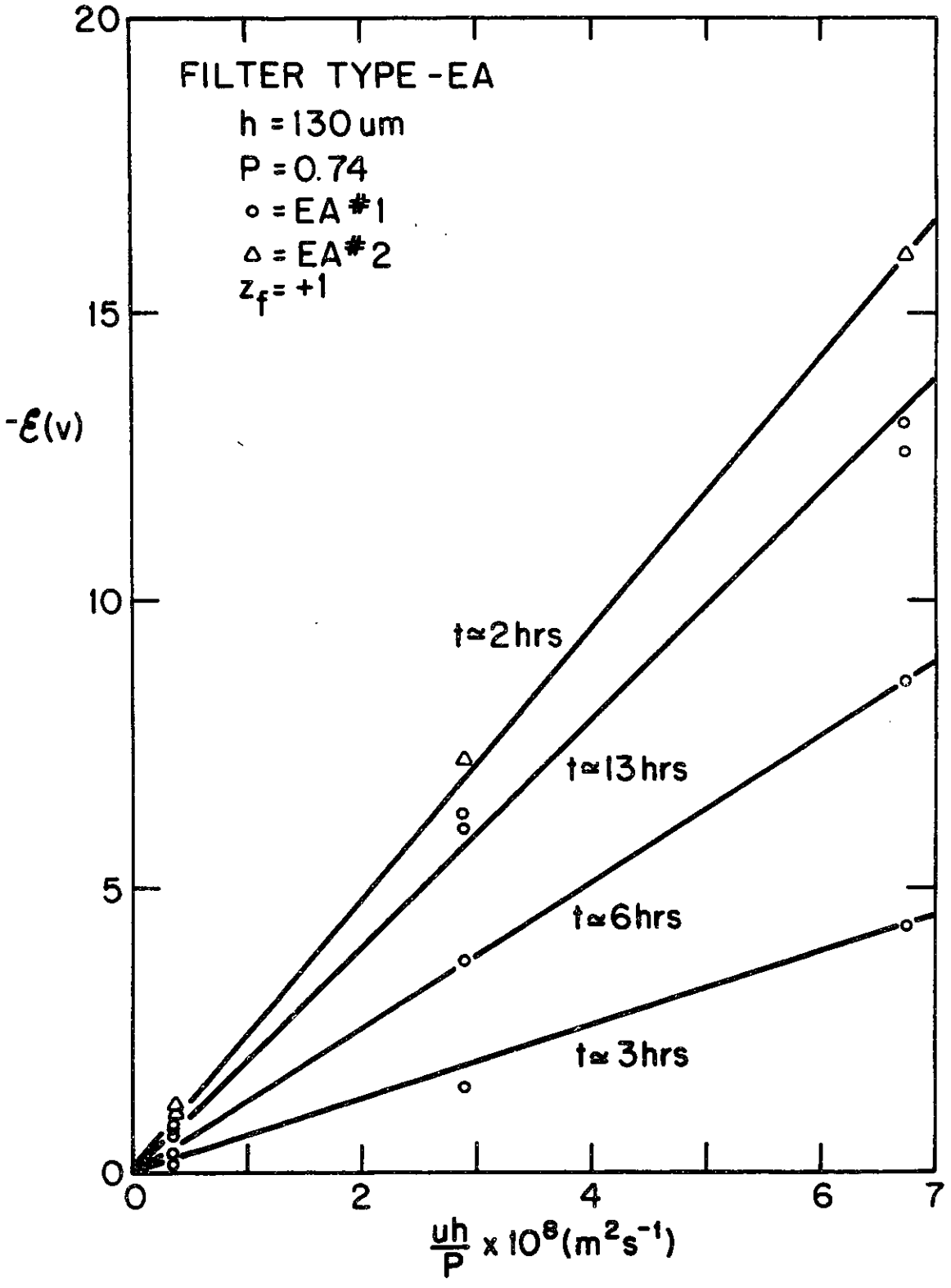


FIGURE 11. Charging emf as a function of reduced flow velocity for EA filters, $\theta \ll 1$.

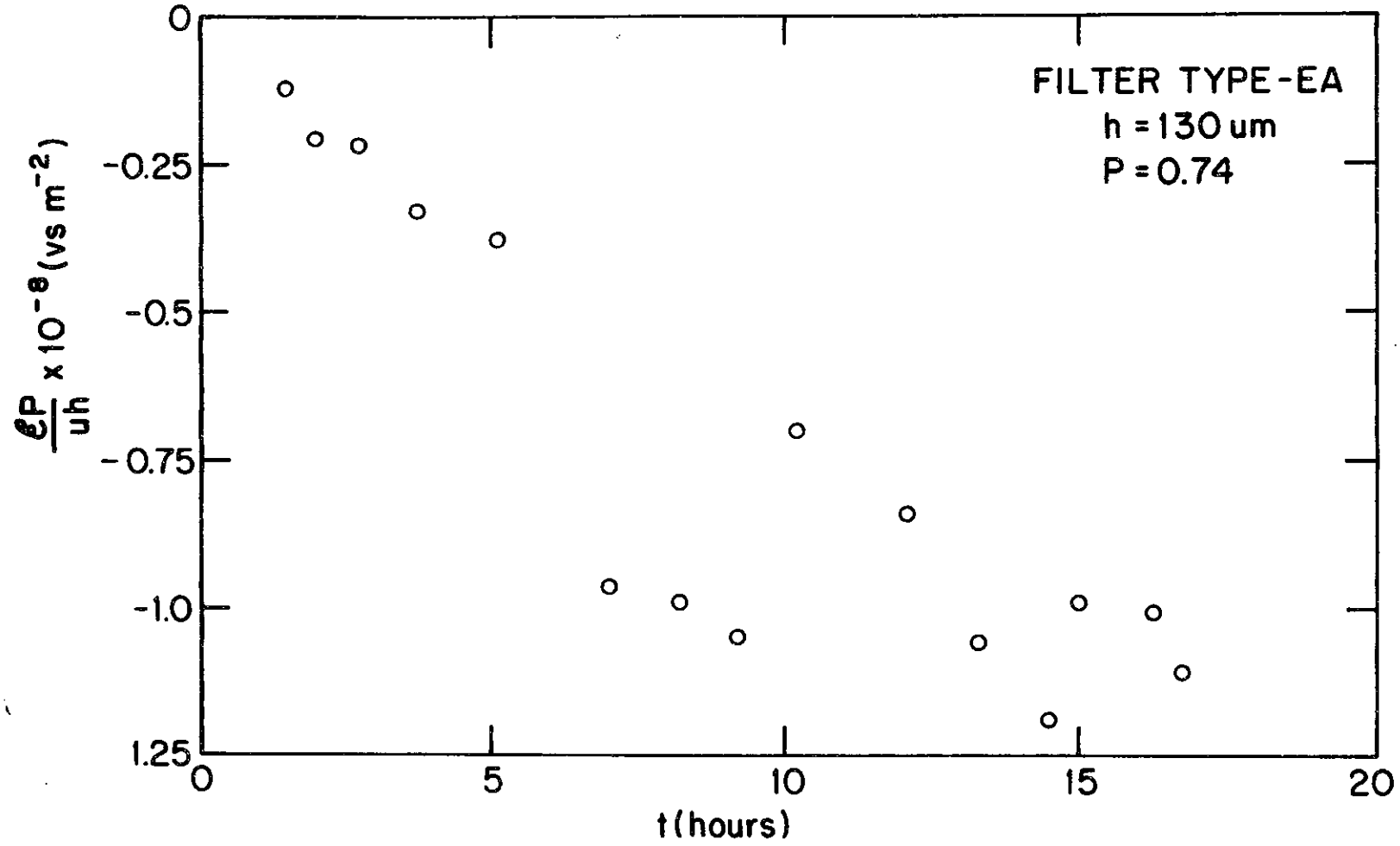


FIGURE 12. Reduced charging emf as a function of hours exposed to flow conditions for EA filters, $\theta << 1$.

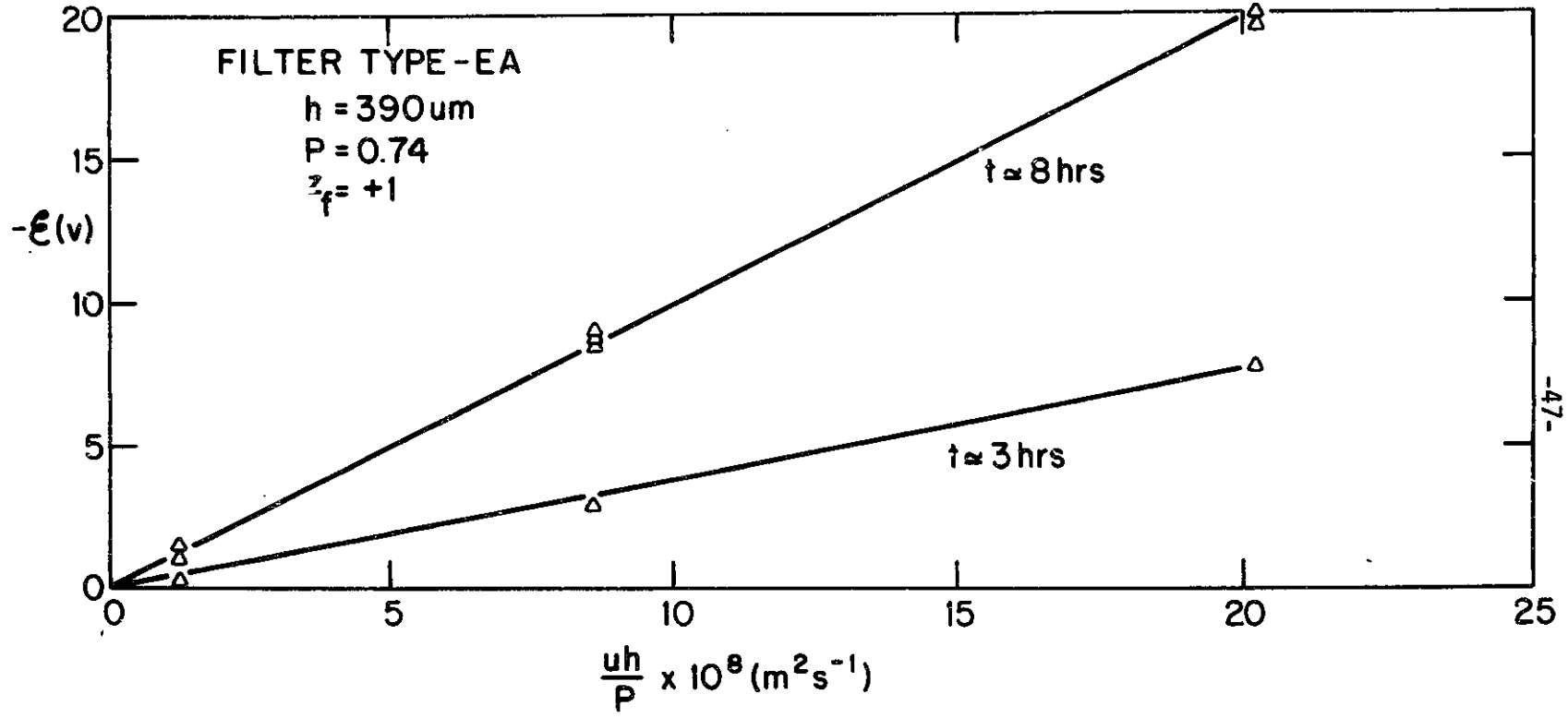


FIGURE 13. Charging emf as a function of reduced flow velocity for EA filters, $\theta \ll 1$.

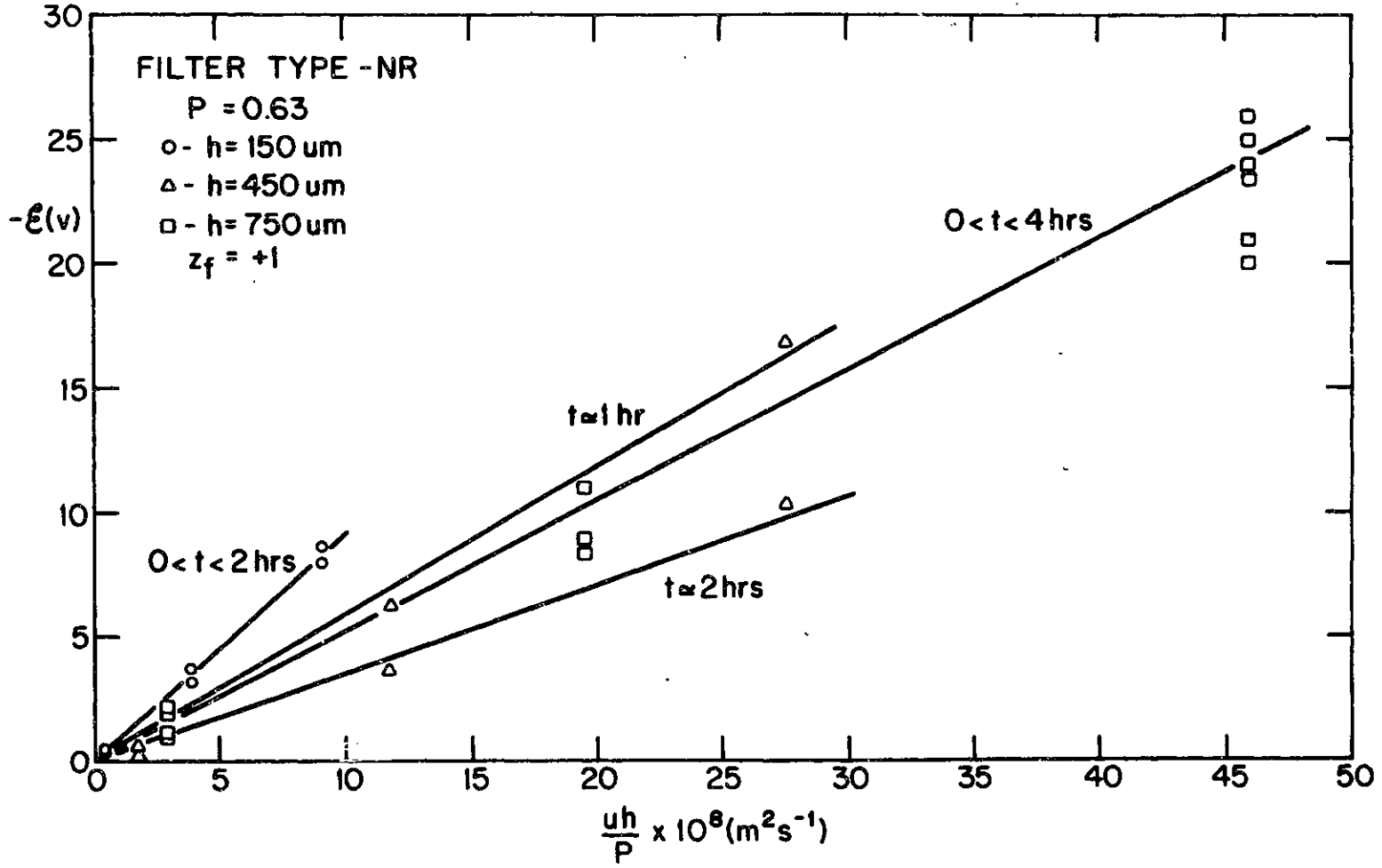


FIGURE 14. Charging emf as a function of reduced flow velocity for NR filters, $\theta \ll 1$.

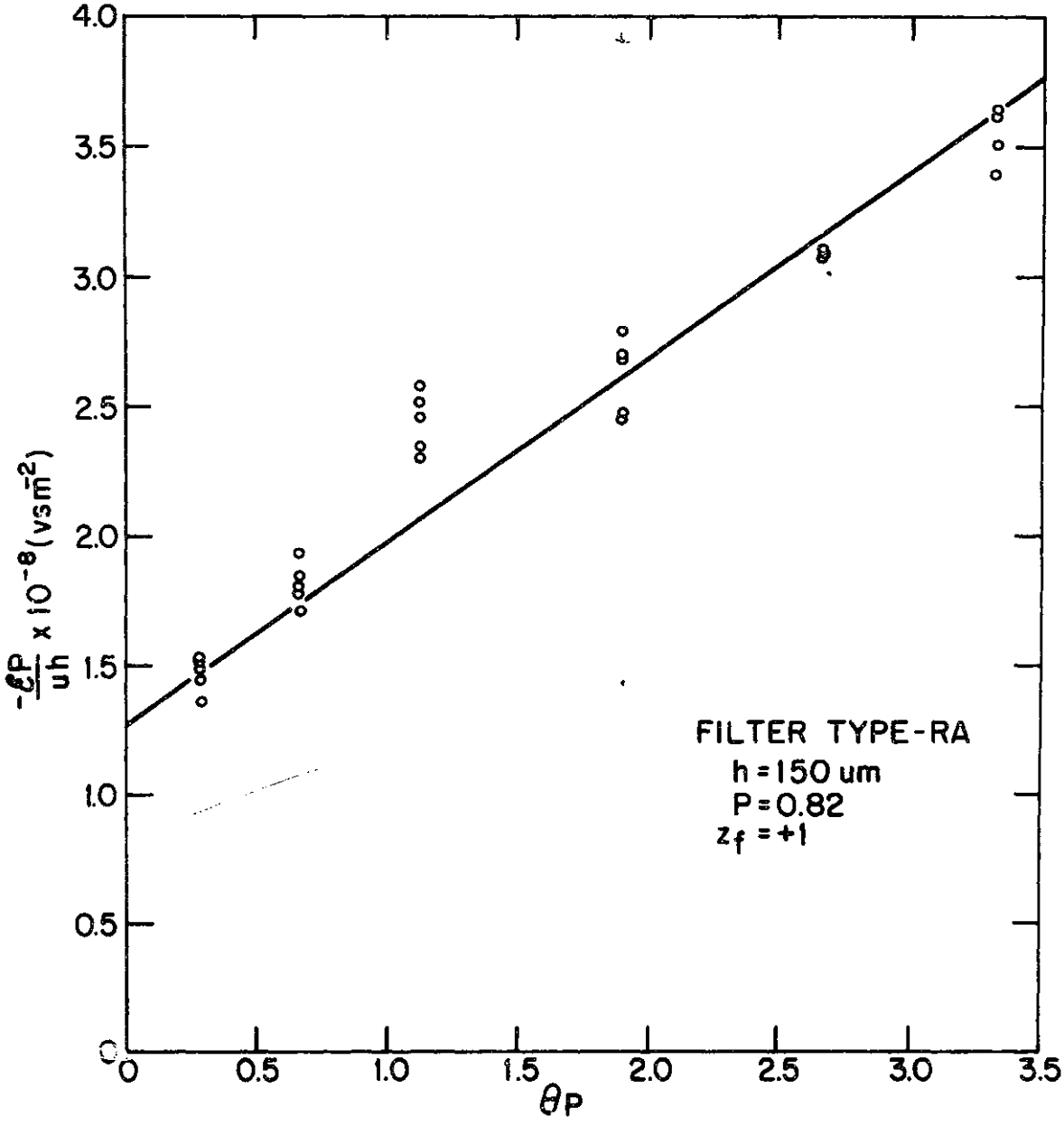


FIGURE 15. Reduced charging emf as a function of reduced flow velocity for an RA filter, $\theta > 1$.

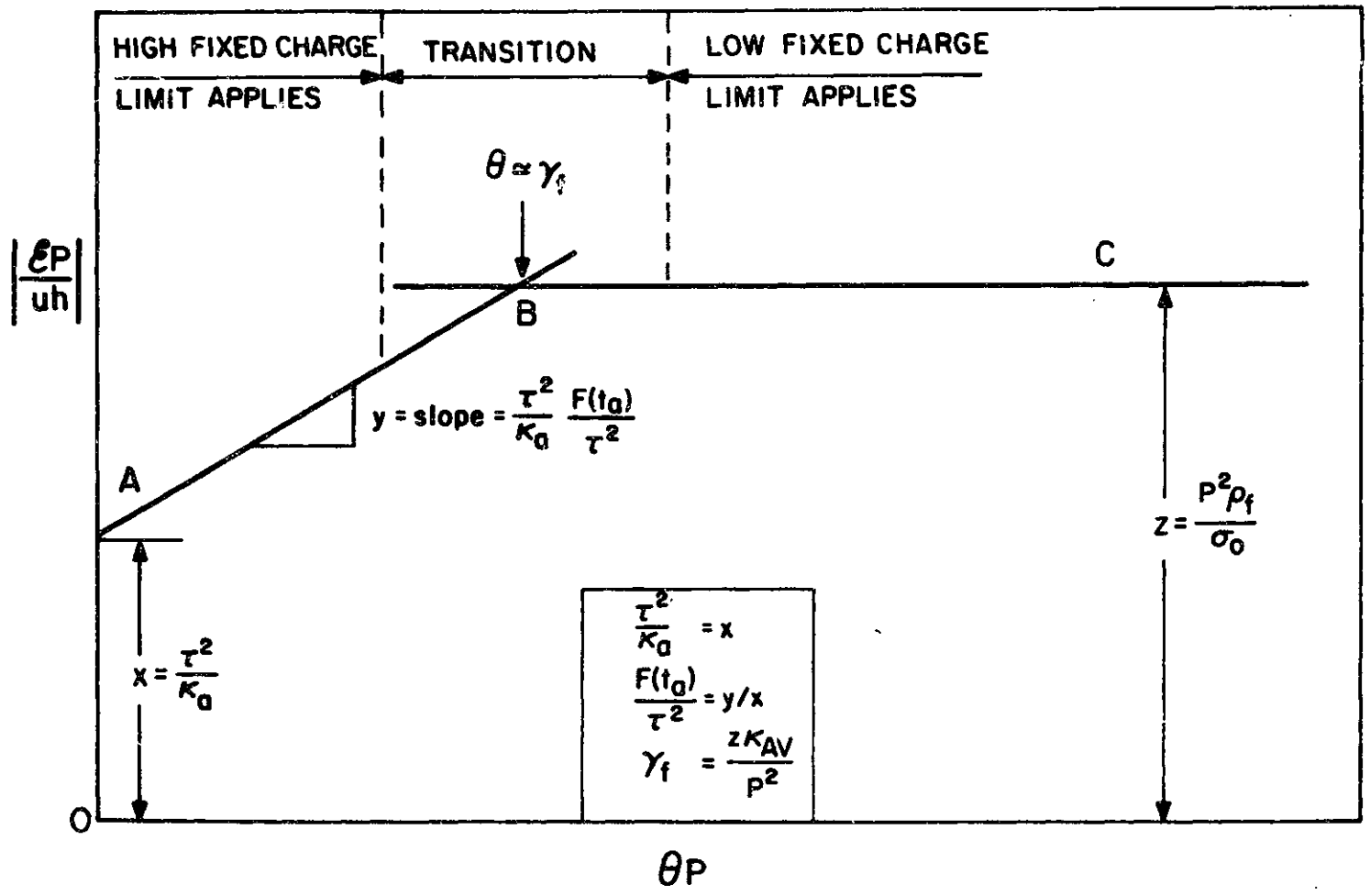


FIGURE 16. Schematic behavior of reduced charging emf as a function of reduced flow velocity for $\gamma_f > 1$.

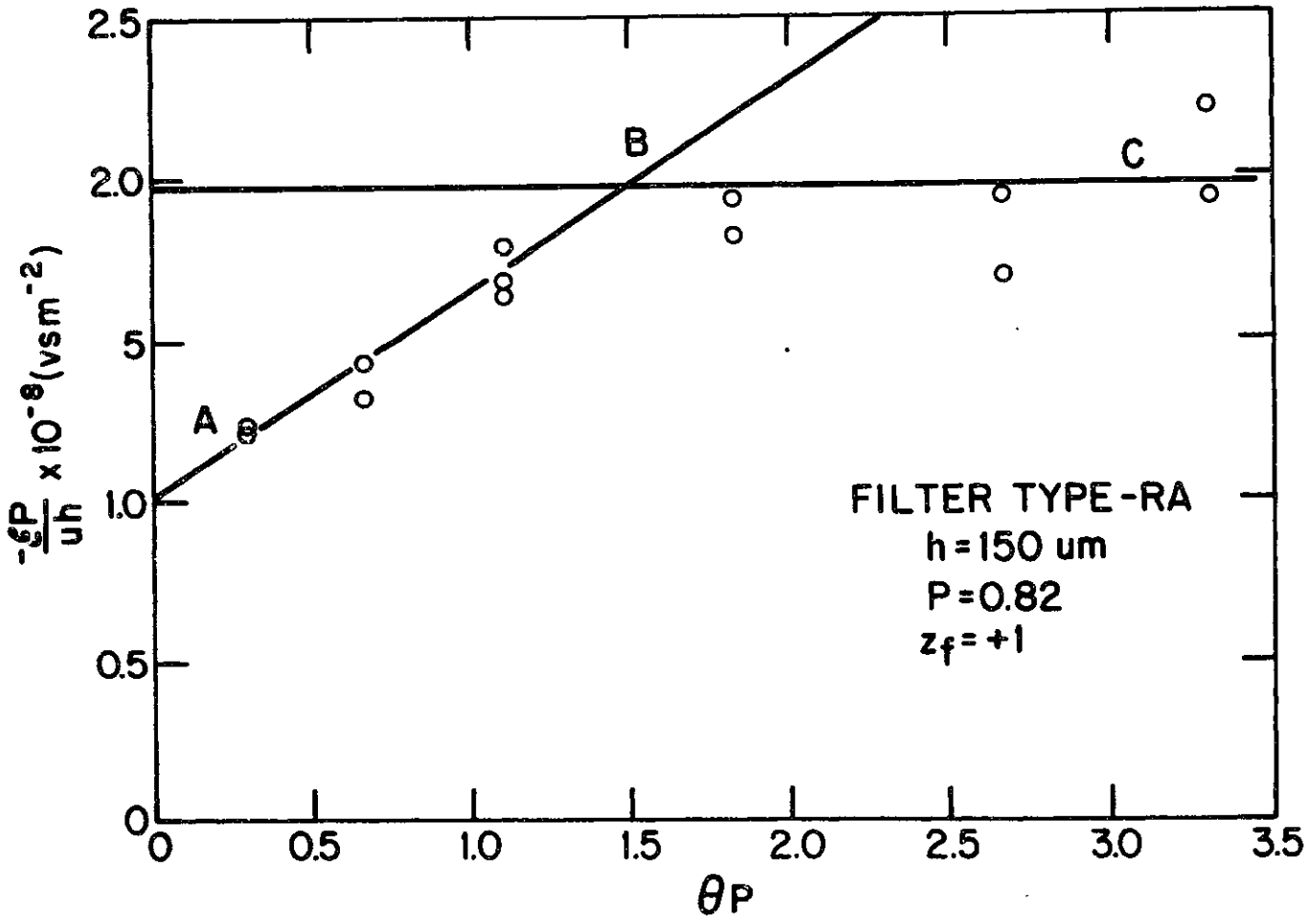


FIGURE 17. Reduced charging emf as a function of reduced flow velocity for an RA filter, $\theta > 1$.

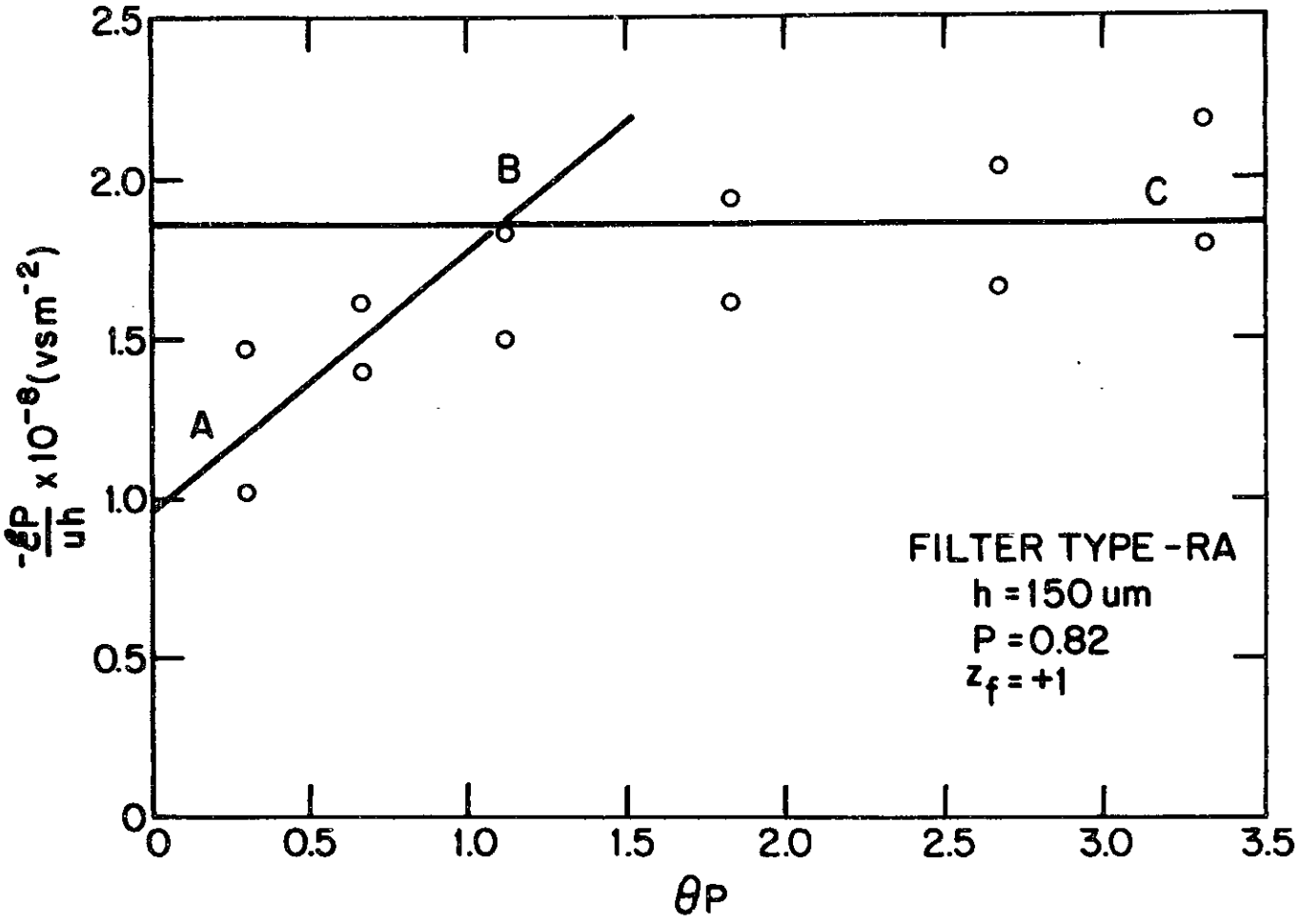


FIGURE 18. Reduced charging emf as a function of reduced flow velocity for an RA filter, $\theta > 1$.

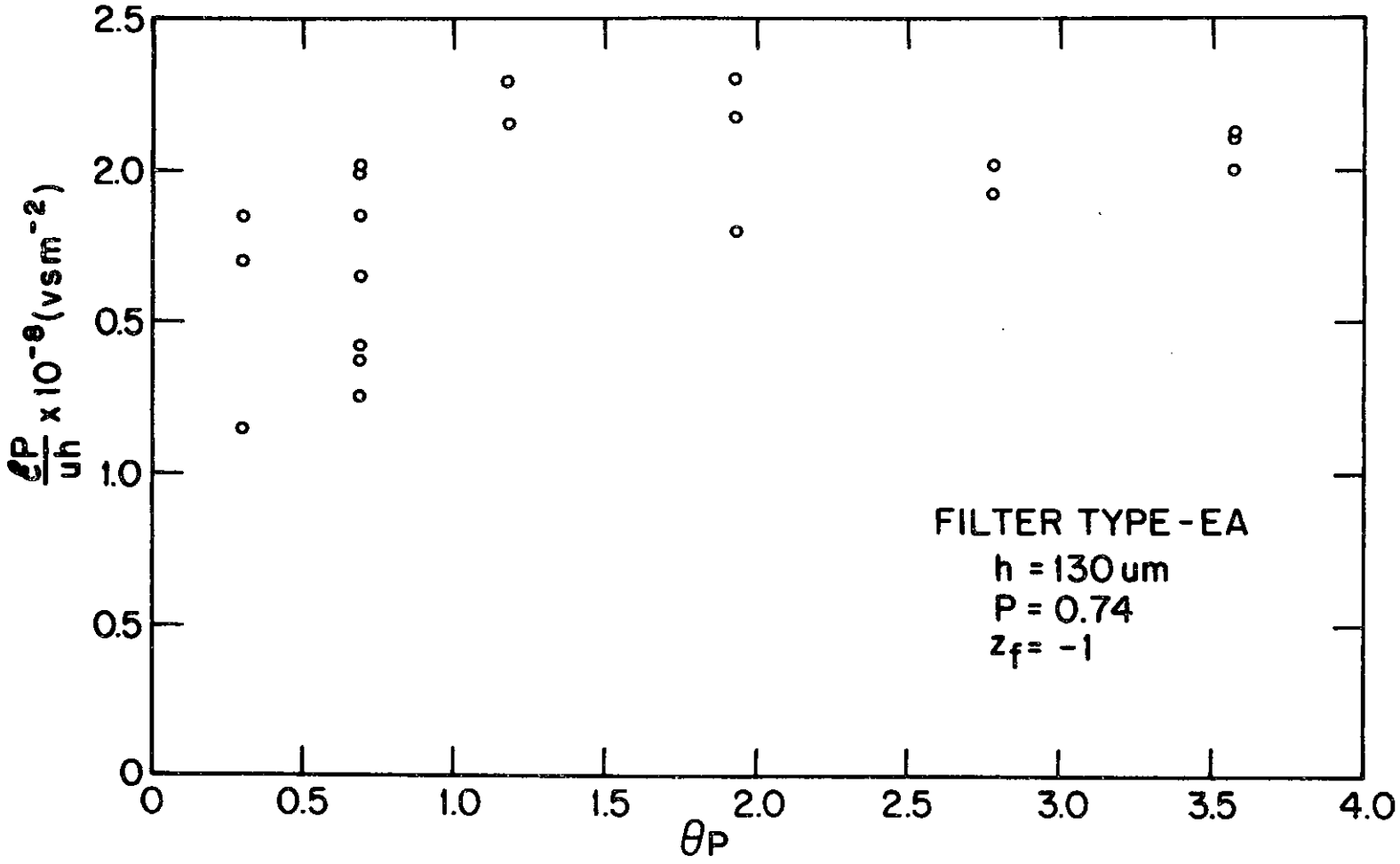


FIGURE 19. Reduced charging emf as a function of reduced flow velocity for an RA filter, $\theta > 1$.